University of Natural Resources and Life Sciences, Vienna

Baugeol. Büro Bauer GmbH, Domagkstr. 1 a, 80807 Munich, Germany

Georgian Renewable Power Company JSC
10 Medea Jugheli Street
0179 Tbilisi
Georgia

Baugeologisches Büro Bauer GmbH
Domagkstraße 1 a
80807 Munich

www.baugeologie.de

Contact: Dr. Peter Neumann
Christoph Wichert

Telephone: +49-89-36040-467
Fax: +49-89-36040-100
e-Mail: Peter.Neumann@baugeologie.de

HPP Mestiachala Priority Projects

Final report on field research and geohazard assessment 2020

Editors: Dr. Sven **Fuchs**
University of Natural Resources and Life Sciences
Institute of Mountain Risk Engineering
Peter-Jordan-Straße 82
1190 Wien / Austria

Dipl.-Ing. Markus **Haidn**
Trumer Schutzbauten GmbH
Maria Buehel-Straße 7
5110 Oberndorf / Austria

Dr. Peter **Neumann**
M.Sc. Christoph **Wichert**
Baugeologisches Büro Bauer GmbH
Domagkstraße 1a
80807 München / Germany

Date: 10th December 2020

Summary and Conclusions

The Final Report on field research and geohazard assessment of the Mestiachala HPP 1 catchment presents the results of the geoscientific evaluation according to the underlying contract between GRPC and our working group.

*The report includes explanatory notes on geoscience and methodology in Chapter 2 and detailed findings from our field campaigns with photo illustration, geographically structured according to the major valleys Murkvami ("Tributary"), Mestiachala and Chalaati (chapters 3 to 5). Base maps of geology and detachment zones in a scale of 1:25,000 (Attachments 1 – 2) as well as geomorphological detail maps of the valleys in a scale of 1:12,000 are attached (Attachments 3 – 5), representing the current mass movement inventory and stability setting that was encountered in 2019 and 2020. A uniform nomenclature is applied for detachment and depositional areas. Interpreting and extrapolating these findings (**event analysis**), present and future geohazards were assessed and filed in detailed geohazard maps of the valleys in a scale of 1:12,500, differentiating rockfall and flow processes in a wider sense (Attachments 6 – 7). Subsequently, geophysical and debris flow modelling as well as rockfall simulation of selected event categories were carried out (chapters 6 – 8). The Attachments 8 – 9 show the respective detailed maps and sections. The high-resolution **impact analysis** in combination with the glacier study (Chapter 9) leads to a precise assessment of the geohazard situation for the HPP 1 (Chapter 10) which is fundamental for subsequent risk assessment procedures. Finally, monitoring requirements to verify dynamics of the geohazard situation are outlined (Chapter 11), which may also be used for possible future warning systems. Feasibility concepts for structural mitigation supplement this report (Chapter 12). Both, monitoring and mitigation are crucial for increasing the safety level of the HPP.*

The results of this study can be summarized as follows. The investigated HPP catchment north of Mestia unveils a window into the Greater Caucasus Mountain range with very steep relief, weak geological zones, glacial over-steepening of slopes, retreat of glaciers and permafrost, leading together with considerable meteorological triggering to a designated mountain hazard environment. Extreme physical conditions are inherent and provide a plethora of different geohazards the catchment is prone to. Consequently, the overall risk level is considerably high and will not be lessened by natural processes in the near future.

The documented hazard situation appears challenging to interpret in the context of risk management, business decisions, mitigation, to name just a few. However, following a hierarchical organization of our findings according to potential hazard volumes (magnitudes), related probabilities of failures (frequencies), regional occurrence and impact modelling, the overall geohazard architecture becomes evident. Simplifying, we distinguish two groups of events. On the one hand, there are numerous, often higher-frequent processes with limited volumes occurring in distinct and predictable locations. We call them "Group 1 events". This heterogeneous group of different hazard types involves rockfalls and slides of low to larger volumes (m^3 to 100s of m^3), debris flows and associated processes with 100s to 1000s of m^3, soil slides and snow avalanches. All these processes have in common that they are of defined

magnitude, can be locally assigned quite accurately (release and runout areas) and mitigated with sufficient efforts. A prominent example is the rockfall area in the northwestern Mestiachala valley flank heading from the gallery north. Here, we have gone a step further and identified high-frequent falling blocks statistically and run a detailed simulation in the area of the gallery and the envisaged new intake, which is the precondition for designing rockfall protection measures. Further examples are debris flow zones or snow avalanches accompanying various gullies and trenches on both flanks of Mestiachala, locally affecting the structures of the HPP. "Group 1 events" have a broad range of frequencies from 11-30 years up to several times per year. To sum up, these events represent a kind of permanent erosion and a mitigation by technical measures, e.g. by flexible rockfall protection fences or protective dams, is possible.

In contrast, the July 2019 mass movement disaster – among other landslides in the region – has shown that less-frequent but higher-magnitude events ("Group 2 events") pose a serious threat to the entire structures of the HPP. Group 2 events include flash flood-like processes following potential water breakouts at the glaciers, e.g. at Lekhziri or Chalaati glacier, or high-magnitude compound processes such as the one originating from the Murkvami valley, in which various types of mass wasting were involved. In addition, we also include potential extensive rockfalls in this second group of events. Voluminous and obviously instable rock towers have been identified west of the nearby gallery (up to more than 10,000 m³). For all of those high-magnitude hazards, which in many cases comprise volumes of several 100,000 m³, it is not possible to forecast accurate and precise timing and mechanical behaviour. However, it becomes evident that they are likely to occur and we have to assume a frequency interval of less than 30 years in the identified hazard areas.

Based on event analytical data, we summarize the major geohazards for the structural elements of HPP 1 as in the table below. The colours/hatchings as well as frequency classifications are explained in Fig. 2-6 in Chapter 2 of the main report.

Table presenting the results of event analysis in the HPP1 catchment (EF 1: >30 years / EF 2: 1-30 years (EF 2.1: 11-30 years / EF 2.2: 1-10 years) / EF 3: ≤ 10 events per year / EF 4: >10 events per year).

Geohazard types and classification / Location / HPP element	„Group 2 Events" low frequency / high magnitude extreme events		„Group 1 Events" permanent erosion processes					
	flash flood	high magnitude compound event	very large	large	rock fall medium	rock fall minor	debris flow	snow avalanche
Intake 1 (original position)	EF 2 several 100,000 m³	EF 2 several 100,000 m³						
Intake 1 (alternative new position)	EF 2 several 100,000 m³				EF 2.1 up to 100 m³	EF 3 up to 10 m³	EF 2 several 1,000 m³	annual
Transit area (penstock, gallery)	EF 2 several 100,000 m³	EF 2 several 100,000 m³	EF 2.1 instable rock towers, up to 12,000m³		EF 2 up to 100 m³	up to 2.5 m³ EF 4 up to 10 m³ EF 3	EF 2 several 100 m³	annual
Powerhouse HPP1	EF 2 several 100,000 m³ *Hazards from Chalaati catchment*	EF 2 several 100,000 m³ *Hazards from Chalaati catchment*						

In order to refine this geohazard scenario and decrease the exposition of the HPP 1, impact analysis on the one hand and monitoring of activity, on the other hand, are essential tools in planning. For this purpose, we have computed and modelled those hazards that directly affect

civil works with either high-frequency (minor/medium rockfall simulation) or with a disastrous effect (high-magnitude debris flow modelling) according to our contract.

Table presenting the applied methods, software and location of impact analysis s.l. in the HPP1 catchment.

	flash flood / high magnitude compound events	rockfall very large - large	rockfall medium - minor	debris flow	snow avalanche
Impact analysis in selected locations	Murkvami tributary **debris flow modelling** *r.avaflow* Murkvami detachment **remote/drone sensing** (geomechanical interpretation) Mestiachala-Lekziri valley **debris flow modelling** *r.avaflow* Intake location **electrical resistivity subcrop modelling** *Res2Dinv* Gallery location **electrical resistivity subcrop modelling** *Res2Dinv*	Transit area zones M-R3b and M-R5b **remote/drone sensing** (geomechnical interpretation)	Gallery / zone M-D4 design event 5,4m³ **rockfall simulation** *GeoRock 2D* New intake location / zone M-D6 design event 8,5m³ **rockfall simulation** *GeoRock 2D*	---	---

With focus on the project priorities and detected key hazards, this leads to the following conclusions:

<u>Conclusion 1:</u> The proximal release zone of the 2019 disaster has not come to a semi-stable state, instead, it is still a highly <u>active</u> area of rock detachment below the retreating Murkvami glacier. We expect repeated events of 100s to some 10,000s m³ in the upcoming years, with potentially high magnitudes (rock failure of up to some 100,000s m³) in a 30-year range. Such a high magnitude event may initialize a disaster cascade comparable to the 2019 event, even reaching Mestiachala valley. Also the Lekhziri glacier front is active and the hazard of a flash flood is given. The glacier study reveals significant glacier retreat in the next decades, resulting in potential high-discharge events.

The effect of such high-magnitude "Group 2 events" on the entire HPP infrastructure, reaching from the intake to the powerhouse are rated as considerable, as we witnessed from the 2019 experience. Debris flow modelling led to the following results of impact showing varying degrees of flow height, pressures and velocities in the sections of Mestiachala valley.

Table presenting Murkvami tributary debris flow modelling (Group 2 events) – Maximum simulated values.

HPP location	Deposition height [m]	Flow pressure [kN/m²]	Flow velocity [m/s]
Former intake1	Up to 18.0-20.0	Exceeding 700	Exceeding 13
New intake1	Up to 4.0	Up to 60	Up to 6

Table presenting Mestiachala valley debris flow modelling (Group 2 events) – Maximum simulated values.

HPP location	Flow height [m]	Flow pressure [kN/m²]	Flow velocity [m/s]
New intake1	In a range of 3.0 – 3.5	In a range of 60 – 70	In a range of 8 – 10
Exposed penstock	In a range of 2.0 – 3.5	In a range of 110 – 125	In a range of 11 – 13
Gallery	In a range of 2.2 – 3.1	In a range of 110 – 135	In a range of 11 – 13
Suspension bridge	In a range of 5.2 – 6.6	In a range of 120 – 250	In a range of 9 – 11
HPP	In a range of 4.0 – 7.0	In a range of 100 – 140	In a range of 8 – 10

<u>Conclusion 2:</u> The western Mestiachala valley rock slope (Dalrakora massif) resembles an active detachment zone, as detected changes between 2019 and 2020 have proven. Minor, medium and also large rockfalls as well as minor debris flows may be released. We have simulated high-frequent rockfalls in two locations and presented all relevant data (design event statistics, energy

classes, bouncing heights, etc.) required for mitigation planning of protective fences. In addition, rock towers prone to large or even very large rockfall volumes were detected in two areas. Since fundamental data are missing, the likelihood and impact can only roughly be estimated up to now.

Conclusion 3: The simulation results of the entire impact analysis (summarized in the tables of Chapter 10), can be used for risk assessment, decision-taking or preliminary-stage designs of countermeasures. We also recommend to re-check the statics and design of existing mitigation structures. For detailed planning, however, among other works, further specified modelling is required.

Conclusion 4: A conceptual framework for monitoring and acquisition of deformation activity has been provided, which is absolutely essential to verify and update the hazard and risk evaluation and which also serves as starting point for possible warning systems. It includes mainly a high-precision survey of the still active 2019 detachment zone of Murkvami valley, regular remote survey of the entire catchment (satellite-based evaluation) and annual on-site inspections of selected locations for assessing stability and activity changes. Only by this means it is possible to detect hidden hazards and risks as well as changes and, thus, adapt planning, monitoring or mitigation, e.g. in respect to currently inactive debris flow channels or exposed rock masses.

Conclusion 5: Based on the presented high-resolution geohazard image, fundamental concepts for risk reduction in case of an envisaged rehabilitation decision by GRPC were drafted. Generally, extensive "Group 2 events" cannot reasonably be mitigated in their total extent, in particular if economic constraints have to be taken into account. However, protective or stabilizing measures along the penstock, the avalanche gallery and further downwards to the right lateral channel banks, the weir, the desander and the powerhouse in combination with regular survey as well as warning systems can increase safety significantly. Key issues are the choice of location and type of intake (e.g. Tyrolean weir), possibly protected by bed load safety nets, or the protection of the penstock and the wider infrastructure against damages by lateral bank erosion using block or reinforced concrete wall support. Scouring of the channel bed can be prevented by groundsills. Sediment retention and check dams can reduce impacts in the downstream HHP structures. Nevertheless, damage to the weir and the desander intake has to be accepted to a certain degree, given the process magnitudes expected. High-frequent rockfalls ("Group 1 events") can be mitigated by protective fences or barriers, which has been proved by our simulations in currently active areas. Additional mitigation requirements against debris flows or rockfalls from lateral detachments or channels has to be revealed by future monitoring as described above.

Summarizing, the basic feasibility of mitigation and thus rehabilitation of the HPP depends on a risk evaluation and finally on risk acceptance by the client, investors, and authorities. Nevertheless, the risk level will remain considerably high since a re-occurrence of mega-events such as the 2019 event is possible and new risks can arise due to significant and fast changes in the high-mountain environment and its balancing factors such as degrading permafrost, glacier retreat and others.

Content Page

Attachments

1 Introduction

1.1 Motivation and assignment

Georgian Renewable Power Company (GRPC) assigned the consortium BBB-TRUMER-BOKU-CRP with a detailed geohazard assessment in the area of HPP Mestiachala (Priority projects, see contract of 02 March 2020). Despite a challenging situation due to the current COVID-19 pandemic, the field campaign was carried out between 10 and 24 August 2020, and comprehensive results were obtained during the mission. Upon request by the Client, an interim report based on the field surveys and preliminary desk-top evaluation of assessed geohazards was submitted on 09 October 2020.

The present final report substitutes the interim report and additionally incorporates, in addition, outcomes of detailed processing in geophysics, modelling, simulation, evaluation of drone imaging and others. The geohazard assessment of the interim report is updated with the results of a high-resolution impact analysis applying debris flow modelling and rockfall simulation. Additionally, an outlook on possible mitigation measures and their influence on safety level is provided, as requested by GRPC.

1.2 Objectives and outline of the report

The objectives of this report are to provide an overview on mass wasting processes and slope instabilities in the entire catchment, as well as to categorize current geohazards with respect to the Priority projects. This geohazard inventory includes a distinction of mass wasting processes, their assumed probabilities of occurrence (frequencies) and of magnitude (volumes), as well as an impact analyses.

In Chapter 2 the geoscientific framework and the overall hazard situation are outlined and the methodology is presented. The following field descriptions of our 2020 campaign will be structured on a geographic level for a better understanding:

- [Chapter 3] Current geohazard situation in the Murkvami valley/"Tributary" (intake 1…),
- [Chapter 4] Current geohazard situation in Mestiachala and lower Lekhziri valley (intake 1, alternative intake 1 position, penstock pipe, gallery, powerhouse…), and
- [Chapter 5] Current geohazard situation in Chalaati valley (powerhouse…)

The subsequent chapters include the detailed processing, starting with an evaluation of geoelectric investigations of the Quaternary Mestiachala valley fill and its subcrop rock topography (Chapter 6), which is prerequisite for software modelling of extensive disastrous mass wasting in Chapter 7. Chapter 8 includes rock-fall simulations and estimations of rock slope

stabilities, whereas the glacier study of Chapter 9 highlights the impact of glacier processes on debris flow or rockfall activity.

Subsequently, in Chapter 10 a comprehensive geohazard assessment is executed by combining and interpreting all these results in terms of probabilities, intensities and impact of natural mass wasting processes. This step sets fundamental parameters for future risk assessment, which is not part of this study.

As additional support for risk analysis, we discuss the significance and possibilities of monitoring (Chapter 11) and give an outlook on feasible mitigation technologies and their efficiency in risk reduction (Chapter 12), which can support future technical and business decisions. The study is finally completed with an outlook on the project (Chapter 13).

2 Geoscientific background and methodology

"Georgia is a country frequently affected by gravitational hazards. According to a (…) landslide hazard map at national scale (Gaprindashvili and van Westen 2016), large parts of the country are classified as zones of medium to high susceptibility to mud and debris flows. The National Statistics Office of Georgia Geostat (2019) counted during the period from 1995 to 2018 more than 10.700 landslides and 3,000 mudflows, causing 50 respectively 93 fatalities as well as damage to numerous buildings and settlements. According to a case study for Georgia (The World Bank 2006), around 85% of the observed debris flow events are triggered by intense precipitation. Next to hydrometeorological triggers, mass movement hazards in Georgia are typically initiated by earthquakes (Gaprindashvili and van Westen 2016). Seismic activity origins from Georgia's location in the convergence zone of the Africa-Arabian and Eurasian plates (Varazanashvili et al. 2012). Research has focused particularly on debris flow disasters in the Central Caucasus, the border region between Georgia and Russia, where altitudes of above 5,000 m. a.s.l. are reached (…). In the Greater Caucasus, debris flows are commonly associated with glaciers. Large-scale events are initiated through the retreat of glaciers, opening for possible debris flows, glacier lake outburst floods or ice-rock avalanches." (WARMEDINGER, 2020, p. 30/31).

2.1 Introduction to the geohazard situation

The July 2019 disastrous event was a compound process resulting in a cascade of different types of mass movements originating from a complex interplay of processes taking place in Murkvami and Mestiachala valley (see Post-Event report, 2019). Even if this high-magnitude compound event was extraordinary in terms of onset and magnitude, the general disposition for similar events and/or event cascades of the entire area is high and therefore, these cannot be excluded. We will discuss these issues in the following chapters. Moreover, minor mass wasting is continuously taking place throughout the entire area (minor debris flows and rockfalls, as well as slides of soil and rock material). Analysing satellite images from multiple years provided evidence that even within the range of some years activity can shift locally, and, as such, an active channel may become inactive whereas others start eroding. A constant "background noise" of mass wasting is present in the entire catchment, the degree of activity (frequency and magnitude) varies between locations. In the present report, such high-frequent processes are summarized as "Group 1 Events" in contrast to disastrous high-magnitude events ("Group 2 Events").

The disposition of the investigated area for mass movements in general is very high, due to factors such as:

- strong relief in a young fold-thrust-belt with extensive detachment zones
- rock masses with mechanically weak zones (multiple faults/thrusts)
- unfavourable structural geology or lithology

The triggering factors are very effective in such a mountain environment and comprise mainly:

- seasonal and daily freeze-thaw cycles
- earthquake accelerations

- heavy precipitation and snow melt
- general retreat of glacier and permafrost

The annual glacier retreat in the region ranges between 10 and 20 m and poses the most prominent impact due to changes of mechanical balance of the oversteepened rock walls (see also glacier study in Chapter 9). This impact becomes quite obvious regarding the observed increase of high-magnitude mass movements in the wider region in the last years or decades. An attempt to summarize such landslides is provided by DOKUKIN ET AL. (2020). One example from the catchment of western Lekhziri glacier is indicated in Fig. 2-4 with assumed several 100,000m^3 of rock and ice. A very large rock-ice-avalanche of assumed 1.2 to 1.5 million m^3 occurred in April 2019 at Bashkara glacier at the Russian - Georgian border just few kilometers to the North (DOKUKIN ET AL. 2020).

In our Report_01 of 09 April 2020 we have documented the ongoing activity in the detachment zone of the Tributary with medium and large rockfalls and debris accumulation. In Report_02 of 10 June 2020 we have suggested a sentry observation of the release area to determine the activity, frequency and magnitude of mass wasting.

2.2 Geology and tectonics

The province of Svaneti geologically is located in the Greater Caucasus fold-thrust-belt, a young Alpidic mountain range, which is characterized by thrust stacking, intense folding and deformation of rock units as well as by normal and wrench faulting. Active fault zones develop according to complex regional stress fields and dissect the mountain range into blocks. Valleys, gorges, rivers and glaciers follow these zones of weakness, like e.g. the tributary or the Mestiachala valley. Details on geological history and structure can be obtained from multiple literature, such as VASEY ET AL. (2020).

The catchment of the Mestiachala river is split in two tectonic units: a northern suite of mostly massive and compact crystalline rocks like granites, granodiorites, gneisses, amphibolites and schists with ages ranging from late Precambrian to Mesozoic (**Main Range Zone**) which are overthrust onto a thick sequence of platy to thick bedded sedimentary rock formations of the **Mestia-Trianeti Zone**. These are mainly composed of dark slates of Jurassic age in the investigated area and generally dip to the North. The thrust contact is a sheared zone of meters or more thickness which trends roughly from East to West and dips northwards under the crystalline rocks (Fig. 2-1). In literature this thrust is referred to as the **Main Caucasus thrust** (MCT).

Geology, rock types and structural conditions can be inferred from the State geological map 1:50,000 as well as from our detailed geological map 1:25,000 in Attachment 1. Additional

information for the catchment area of the Mestiachala HPP 1 is described in the geological report by Geoengineering Ltd. (2015).

Fig. 2-1: Left: Image from helicopter flight showing the MCT in the tributary (detachment area of 2019). Inset shows simplified sketch transect with main units of the Svaneti Great Caucasus (from: Vasey et al. 2020). The blue rectangle shows the position of the Mestiachala HPP 1. Right: view to the NW (image obtained from: https://pereval.online/object/2812#image-2).

The following rocks and formations occur in the study area (Tab. 2-1). Typical rock appearance in the Mestiachala HPP 1 catchment is shown in Fig. 2-2.

Tab. 2-1: Rock units and their stratigraphic framework in the Mestiachala HPP 1 catchment according to state geological map 1:50,000 and Geoengineering Ltd and other sources.

Major stratigraphic / tectonic unit	**Geological age**	**Formations / Rock suites according to State geological map 1:50,000**	**Rock types HPP1 catchment according to the present study**
Post-thrusting depositional systems and volcanism	Quaternary – Neogene	Q alluvial and glaciogenic deposits *(not differentiated here)* ΦN volcanic dikes and veins	Various deposits *(see attached geological and geomorphological maps)*
Main Range Zone	Mesozoic	Intrusives (plutonic rocks of Ushba Massif): βJ_2 Middle Jurassic gabbro-diabases, diabase-porphyrites and granitoids	Diverse plutonic rocks *(as deposits in Chalaati valley)*
	Late Paleozoic	Intrusives (granitic and gneissic rocks): $y_1C_1^2$-C_2 – Early and Mid-Carboniferous porphyritic granites. yD_3-C_1^1 – Late Devonian and Early Carboniferous plagiogranites and quartz diorites.	Gneisses Granites
	Early Paleozoic – Proterozoic	Basement (metamorphic and migmatic rocks): O-S_1dl Ordivician-Silurian Dolrinskaya Suite, crystal schists, amphibolites and migmatites	Amphibolites Phyllites
Mestia-Tianeti Zone	Mesozoic	$J_1^2ms_2$ – Lower Jurassic Zedamuashi sub-suite. Siltstones, slates, schists sandstones (350-500 m).	Claystones / Slates Quarzites

Fig. 2-2: Typical rock appearance. Left: Lower Jurassic slates (Zedamuashi Member) with pronounced cleavage at gallery location. Right: Late Paleozoic banded gneisses in Mestiachala valley.

During our field investigations we have documented lithologies and their engineering geological properties such as strength, weathering and fabric. Discontinuity sets were documented (e.g. bedding, cleavage, joints, faults), which occur as large lineaments on satellite images and as cracks or cleavage in the outcrop. The main types and directions are indicated in Attachment 1. These data have been included in our stability considerations of rock slopes, since such discontinuities are critical failure planes, e.g. the cleavage along which also the event of July 2019 was initiated. The major sets have already been presented in our Post-event report of 2019.

Remark: Detailed engineering geological classifications, as well as petrographic, structural and geomechanical studies were performed and their results are documented, but are not key subject to this report and would blast it. Information will be supplied where needed in terms of hazard assessment.

2.3 Seismics

The Great Caucasus fold-thrust-belt is an active orogen. Large lateral fault systems and thrusts like the MCT are a source of repeated earthquakes, which mirror the release of tectonic stress. A detailed seismic hazard analysis has been presented by Geoengineering Ltd. (2015).

In our Post-event report (2019) we have pointed out monitored seismic events on 25 July 2019. It is clear that such triggers will reoccur frequently and increase the hazard of future rock failures

2.4 Geomorphology and glaciers

The study site is located in a high-mountain environment and, as a consequence, is influenced by periglacial conditions and glacier retreat (Fig. 2-3). A mean glacier retreat of 8.1 ma^{-1} has been reported for the Caucasus between 1985 and 2000 (STOKES et al. 2006). Supraglacial debris cover is known to have an important influence on glacier mass balance primarily through its influence

on ablation, but also as a source of material prone to different mass wasting processes. Glaciers and geomorphology have been evaluated during the 2020 field campaign based on a preparatory desktop analysis of satellite imagery and available scientific literature as well as reports originating from the HPP planning and construction phase.

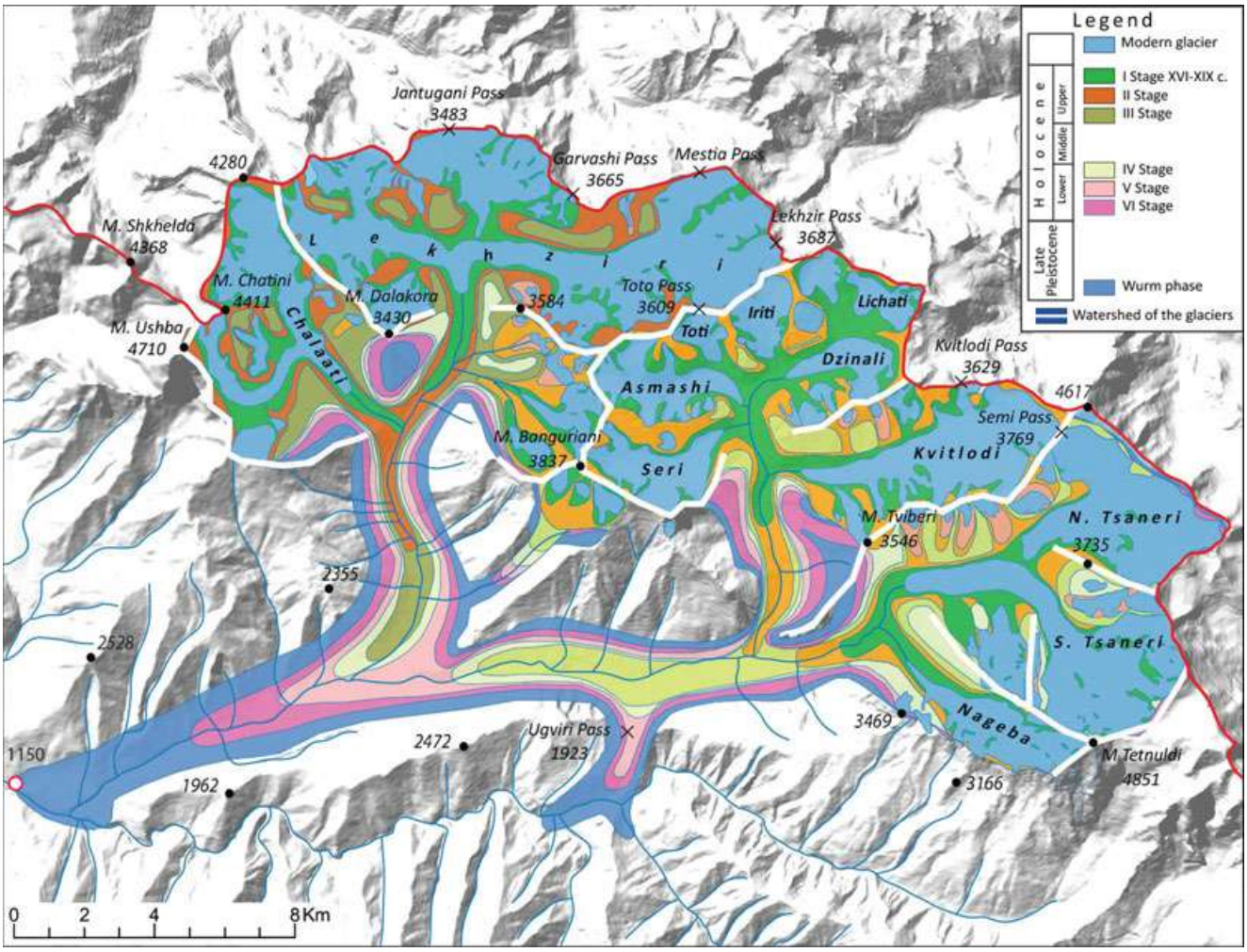

Fig. 2-3: Late Pleistocene and modern glaciers in the Mulkhura and Mestiachala River gorges (TIELIDZE 2017)

2.5 Methodology and data acquisition

For our geohazard assessment in 2020 we applied various multidisciplinary investigation steps and methods.

Field works / targets (locations displayed in Fig. 2-4):

- Geomorphological / geological / structural mapping of valleys and slopes
- Drone imaging campaigns
- Large field trips – Chalaati – Murkhvami and partly Lekhziri valleys
- Investigation of detachment zone 2019 – new insights into stability situation
- Investigation of rock-fall detachment areas in Mestiachala valley

- Determination of rock-fall event sizes (block size statistics)
- Determination of travel paths of rock-falls and activity distinction
- Characterization of valley fills, alluvial fans and mass movement deposits
- High-resolution geoelectrical transects, insight in basin morphology
- Hydrological measurements
- Glaciological investigation

Desktop / Laboratory works / Evaluation:

- Multitemporal satellite image analysis – remote geology/geomorphology (Pléiades satellite imagery of 06 September 2014 and 31 August 2019, SPOT6 scene of 01 August 2017)
- Debris flow modelling with software *r.avaflow*
- Rockfall simulation with software *GeoRock 2D*
- Large rock slides – geomechanical model approach
- Glacier study
- Evaluation of photo archive (helicopter survey of 27 August 2019 etc.) and documentation of RP Global's subcontracting consultants and US Aid as well as available scientific publications

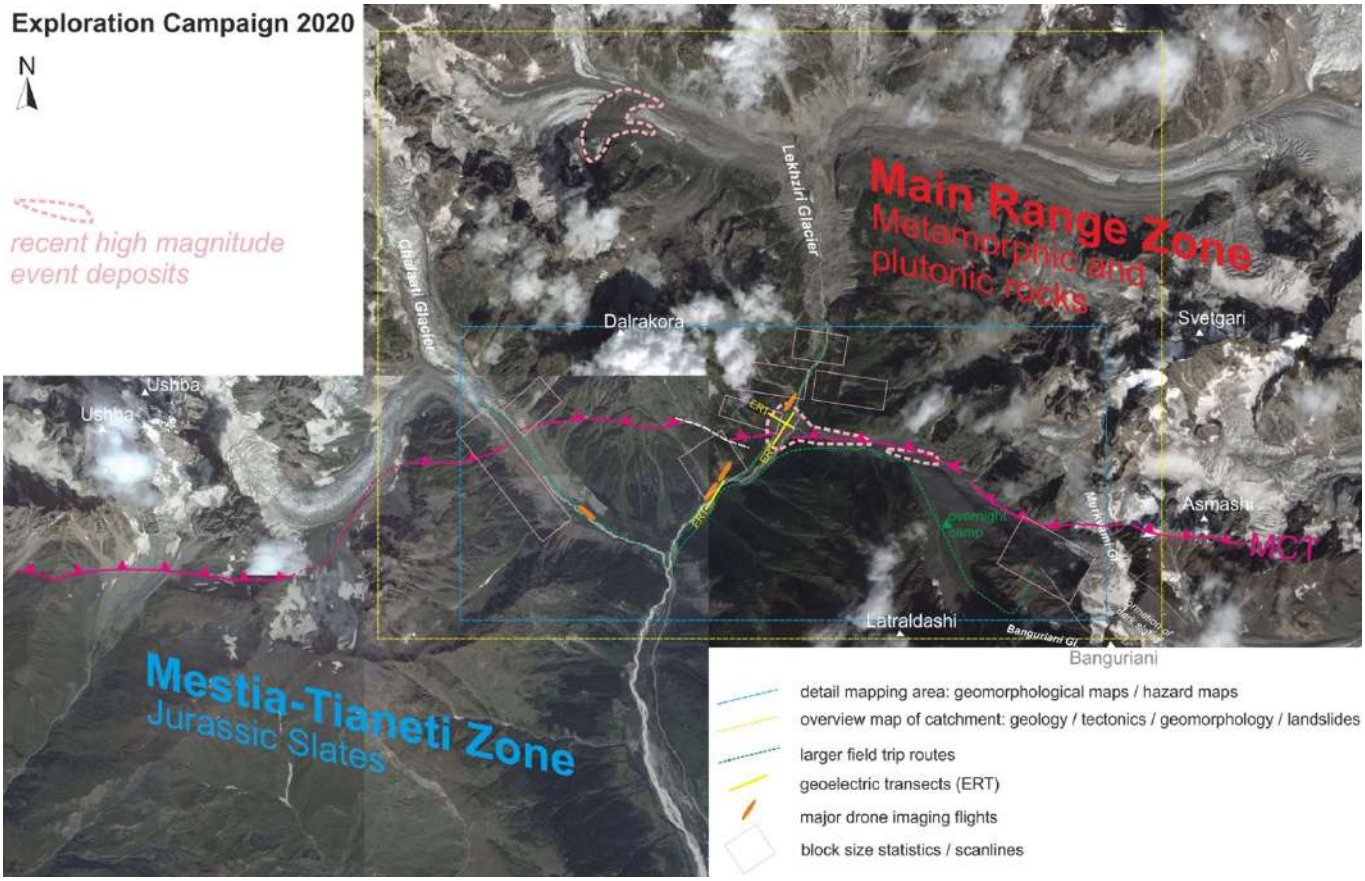

Fig. 2-4: Satellite images of the working area showing the trace of the Main Caucasus thrust MCT with main tectonic units as well as the mapping area (blue hatched line) including special investigation sites (lower left image obtained from: https://pereval.online/object/1963#image-9)

General remarks:

Locations in the text are provided with UTM coordinates (zone 38T) for orientation. In addition, we indicate detachment (release) and depositional areas as well as debris flow areas with consecutive numbers to be found in the attached maps.

Tab. 2-2: Nomenclature and abbreviations applied in the present report and attached maps.

	Major location/valley		Depositional areas		Release / detachment zones
T-	Tributary	**-D**	Rockfall deposition area	**-R**	Release area of mass flows
M-	Mestiachala	**-df**	Debris flow runout area	**-Ice**	Glacier ice remnants
C-	Chalaati	**-**	-	**-**	-

2.6 Processing geohazards and applied classification

The processing of geohazards, their classifications and definitions of this study follows rules of national and international hazard-related risk management.

Processing: Geohazard assessment (Fig. 2-5) in a wider sense consists of two main steps, namely the event analysis, in our case as a result of mapping and field evaluations of 2019 and 2020, and the subsequent impact analysis as a result of modelling of specific hazards (i.e. high-magnitude debris flow modelling). While the event analysis defines the crucial scenarios and their corresponding likelihood of occurrence as well as volumes at risk, the actual hazard intensity and the extent of the hazard are determined in the impact analysis.

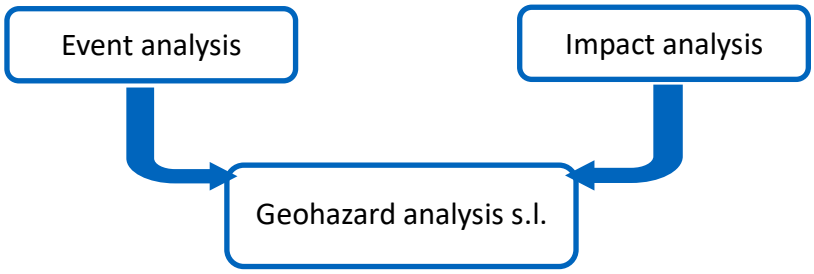

Fig. 2-5: Workflow of the geohazard assessment.

In high mountain environments with multiple hazard sources emphasis has to be given to event analysis of field gathered and remotely sensed data. Large parts of our geohazard assessment are thus based on this event analysis step (also our presentation in the Interim report of 09 October 2020). Specific hazards defined in this preceding event analysis, however, have to undergo an additional impact analysis, in which the extent and intensity are identified by numerical simulations and modelling. According to contract we have done this in respect to high-magnitude cascading events such as the one from the Tributary, and to higher-frequent channel-based (debris flow) processes and rockfalls. The intensity is specified based on the flow depth, flow velocity and temporal onset of debris flows or on runout and bouncing heights of blocks.

These investigations are essential since e.g. a high-magnitude triggering event in the starting zone may not necessarily result in extraordinary loss at an element at risk located in the run-out area.

Applied classifications: In general, our **geohazard ratings** result from the combination of frequencies and magnitudes/intensities of observed and documented events as well as possible future events. The approximated occurrence probabilities (low…very high) refer to the evaluation of **activity indicators** in the field (e.g. fresh blocks, tilted trees…) and disposition factors (e.g. open cracks, joint orientation…) since data on observational records and event inventories were not available. Probabilities are indicated as far as possible as long as scientifically sound.

In the following, these probabilities are expressed as recurrence frequencies in reference to the Austrian Code ONR 24810. This Code is a frequently applied and reliable guideline for hazard assessment, design and implementation of mitigation measures.

The following colours and signatures (Fig. 2-6) are applied to indicate and characterize geohazard zones in the catchment, as presented in the Geohazard Maps of the Attachment 6 and Attachment 7.

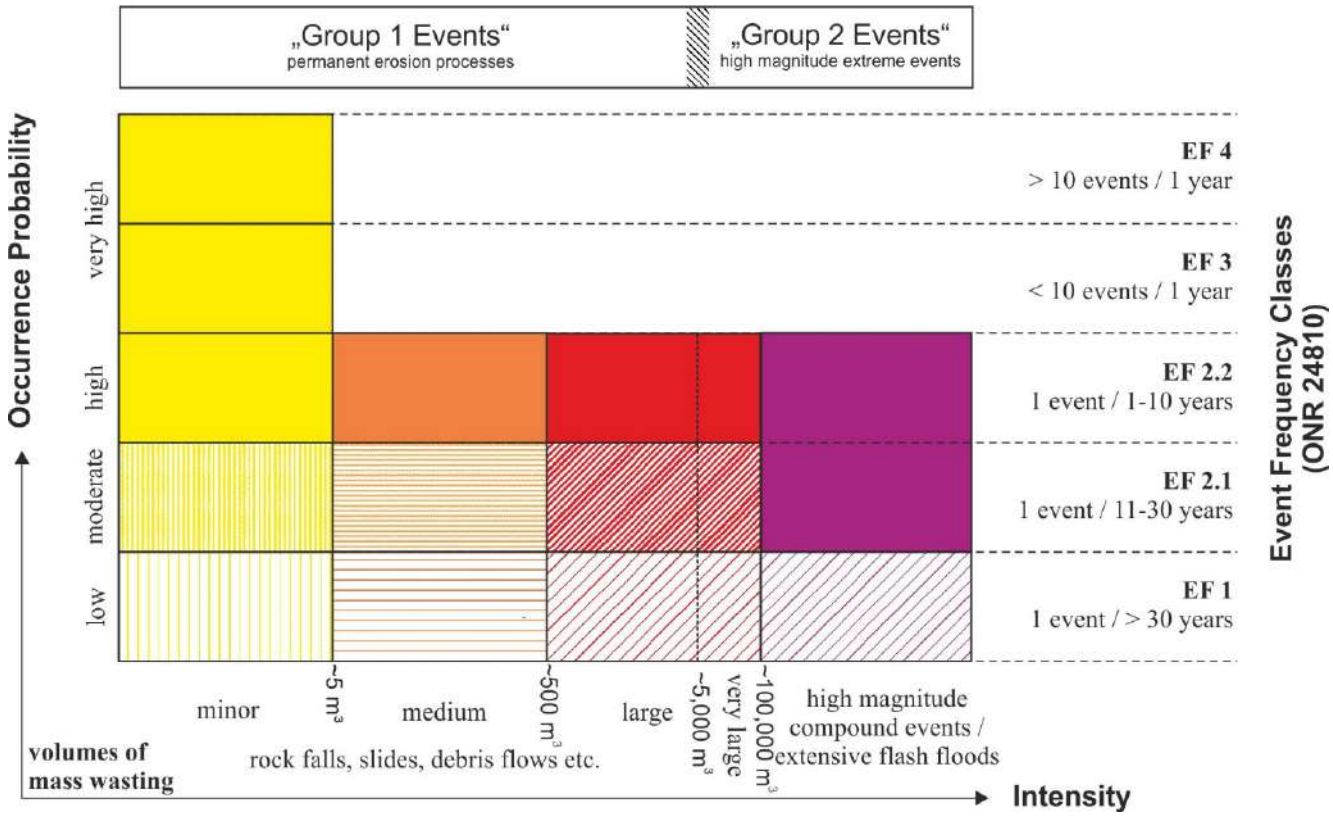

Fig. 2-6: Geohazard matrix for mass wasting processes differentiating volume (intensity) and frequency of rockfalls, slides, debris flows and larger mass wasting processes (flash flood-like events and high magnitude compound events such as 2019). Classification based on ONR 24810 with minor adjustments.

Presentations in maps:

The results of our analysis are presented in plans and maps.

- ⇒ Geoscientific database (Attachment 1 to Attachment 5 and Attachment 9): In the Attachment 1 and Attachment 2 we present base maps of the entire catchment in scale 1:25,000 showing geology, tectonics, major landslides and the principle detachment zone classification. Attachment 3 to Attachment 5 show detailed results of geomorphological mapping along the main valleys Chalaati, Mestiachala and the Tributary. Attachment 9 includes geophysical exploration results of the Mestiachala valley.
- ⇒ Geohazard maps (Attachment 6, Attachment 7 and Attachment 8): The Attachment 6 and Attachment 7 present the results of the event analysis, distinguishing rockfalls and flow processes over the entire investigated area. Attachment 8 presents detail maps of debris flow modelling (impact analysis) for specific areas.

In the following (Chapter 3 to 5), we summarize our main findings on mass movements and provide an inventory.

3 Recorded situation of Murkvami valley ("Tributary")

3.1 General data

The left tributary of Mestiachala river spans between 1940 m asl and 3838 m asl and covers an area of around 1.2 hectares. It is characterised by steep mountain topography with glaciers covering the upper part of the catchment (Murkvami glacier in the NE and Banguriani glacier in the S, divided by a ridge originating at Mt. Banguriani (3838 m asl) and the large middle moraine between the Murkvami and Banguriani glaciers). Current lateral moraines which are equivalent to those in the European Alps at the end of the so-called Little Ice Age in the 1850s can be observed in the catchment as well as in surrounding valleys (KHAZARADZE et al 2018). Since then, glaciers were retreating with a reported speed of tens of meters per year (Tielidze and Wheate 2018), which was also the observation in Chalaati valley (see Chapter 5). Glacier slope may also play a significant role in determining glacier area change, i.e. the steeper the glacier, the larger the area loss observed. The rate of glacier retreat is, however, regionally variable and depends on local factors such as orientation, inclination and altitude, and therefore mass balance, glacier geometry and topography of the underlying bedrock, and debris cover (see also Chapter 9). The valley bottom is covered by deposits originating from (a) unconsolidated ground moraine material of different geologic origin, and, most prominent, (b) deposits of multiple types of mass movements including the Mestiachala 2019 event.

The geology and tectonic structure of the valley is defined by the West-East-trending Main Caucasus Thrust, which emplaces massive gneisses (crystalline rocks) onto Jurassic Slates (see Attachment 1). A steep shear zone with friable slates has developed, along which the shaping of the valley by glaciers occurs.

The detailed results of field investigations and event analyses, distinguishing the 2019 event as well as rockfalls and flow processes over the entire investigated area along the Tributary valley are described in the following Chapter. Additionally, geomorphological maps and geohazard maps are attached (Attachment 5, Attachment 6 and Attachment 7).

3.2 Mass movement inventory

The entire valley bottom is covered by residual masses from the 2019 event, with an average width of 200 m and a superelevation of up to 60 m on the northern slopes, the latter with steadily decreasing thickness in upslope direction. Both, the southern and northern slopes in the lower part of the valley are formed by older rockfall deposits with only minor evidence of recent activity in most areas and only minor parts of an active type with frequencies of 11 - 30 years (EF 2.1) or locally higher. These may not significantly provide material to the channel for further erosion and transportation downwards.

Some gullies are detectable on the northern slopes; these provide occasionally material through debris flow-type processes (hillslope type), such as the larger fan T-df1 (E319,500, N4,776,800). These deposits may become available for erosion during larger mass wasting processes along the valley bottom/Murkvami channel, nevertheless, magnitudes may be in a range of < 7,000 m³.

Major sources for potential erosion are deposits originating from the 2019 event (T-R1b,c) located along the valley bottom, three major deposits can be distinguished. These include from west to east the area T-D1a (E318,200, N4,776,922) with a total volume of approx. 100,000 m³ (240 x 40 x 10 m) next to bedrock at the left (southern) river bank, area T-D1b (E318,512, N4,776,845) with a total volume of approx. 180,000 m³ (290 m x 60 m x 10-12 m) at the right (northern) river bank, and the dominant deposition T-D1c (between E318,950, N4,776,747 and E319,777, N4,776,615) along the right (northern) river bank opposite the mouth of Banguriani valley at the lower terminus of the middle moraine (total volume approx. 800,000 m³; 800 m x 70 m x 15 m with a distinct scarp towards the hillslope, Fig. 3-1 and Fig. 3-2). These deposits will definitely become major sources of material intrusion into any debris flow-like or other channel-bound discharge process as well as any cascading process which is comparable to the 2019 event, depending on magnitude and transport capacity.

Fig. 3-1: View along the Murkvami valley bottom with large sediment deposits (T-D1c) of the 2019 event and debris flow fans on the northern side. View to the east.

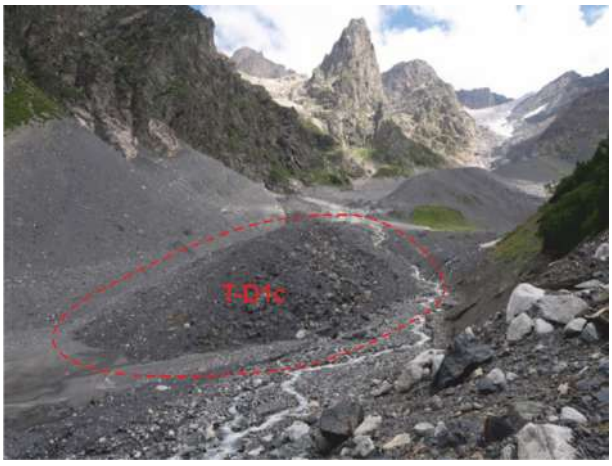

Fig. 3-2: Major sources for potential erosion are deposits originating from the 2019 event located along the valley bottom (here T-D1c). View to the east.

The landscape-forming large middle moraine of Murkvami and Banguriani glaciers, originating from the so-called 1850 extent, is relatively stable and was not significantly eroded by the 2019 event. Material is composed from typical moraine deposits of different debris types ranging from silt-sized glacial flour to large boulders. The debris is typically sub-angular to rounded in shape, and covered by a veneer mainly composed of the phyllitic deposits from the 2019 event.

In the upper part of the valley, three distinct sections with debris-covered dead ice (T-Ice) are detectable (E320,180, N4,776,112; E320,292, N4,776,106; E320,476, N4,775,982) with a volume

of approx. 1,800 m³, 2,500 m³ and 17,000 m³, the latter being of high relevance for future mass movements due to the axial position with respect to the channel as well as the ice content, which considerably reduces friction of any gliding or flowing mass and may therefore lead to an increase in speed of mass movements. Additionally, minor debris flow channels (T-df2, T-df3, T-df4, T-df5) feed some loose material from the north with high activity but small magnitudes, depending on snow melt and precipitation.

Rockfall activity in the northern and southern slopes increases in the upper part of the valley. The general activity of minor rockfall is estimated in classes EF 3 to EF4. The release areas of the 2019 event is discussed in Chapter 8.2.1.

Deposits of the latest rockfall can be detected on the glacier surface T-D3 (between E321,188, N4,775,604 and E321,345, N4,775,449, Fig. 3-3) with an extent of 210 m x 50 m x 2 m (> 20,000 m³), this material will immediately become available for erosion once the glacier retreats further at the current annual rates of 10-15 m.

Another source of material are the rockslide deposits (T-D2) in the western part of the crest between E320,702, N4,775,767 and E320,820, N4,775,551 with an extent of 250 m x 70 m x 2-3 m and an approximated volume of 35,000 m³-50,000 m³.

Fig. 3-3: View towards the glacier tongue of Murkvami glacier and part of the latest rockfall deposits T-D3 on top of the glacier surface. View from above to the north.

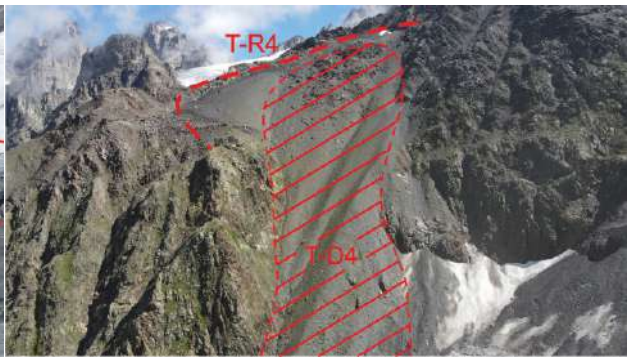

Fig. 3-4: Deposition and release area (T-D4, T-R4) of the landslide on the northern flank of Banguriani valley. View to the northeast. (© Sebastian Resinger)

The landslide located on the northern flank of Banguriani valley (T-R4, T-D4) with 360 m width and 400 m length (Fig. 3-4) is traceable over years, and sliding velocities are within a range of decimeters per year, as such, a hazard for channel processes has been excluded in the current survey. Nevertheless, if major parts of the ridge between the two valleys collapse, the material may become available for further transport downhill and possible mass wasting processes.

From satellite images the release zones of rock masses and glacier ice in July 2019 can be determined (Fig. 8-15). During our field trip this image was verified and investigated in more detail. Critical release areas are T-R1 and T-R2 which were active in 2019. The following images show the most prominent detachment zone T-R1 of 2019 and the steep rock face as a probable

future detachment (T-R3). Further details on the rock mechanics and structural geology are presented in Chapter 8.2.1 In summary, we want to emphasize the high probability for future large rock slope failures which have been indicated on the map in Attachment 2. The occurrence probability is assessed as EF 2: 1-30 years.

Fig. 3-5: Detachment areas T-R1 and T-R2 of the 2019 event zone and future release area T-R3. View to the northeast.

Fig. 3-6: Left: Northward view to crystalline rock towers of Main Range Zone at the northern margin of the tributary with multiple minor rockfall detachments and active cracks along which medium or large volumes might detach in the future (see also Attachment 1). Right: Detachment areas T-R1, T-R3, T-R4 and T-R6 and deposition area T-D4. View to the northeast.

4 Recorded situation of Mestiachala and lower Lekhziri valley

4.1 General data

Geomorphology and natural hazards were assessed for Mestiachala river at a length of 3,900 m, a trajectory between HPP 1 and approx. 800 m above the 2019 event deposits. The valley bottom is covered by deposits originating from (a) unconsolidated ground moraine material of different geologic origin, (b) deposits of multiple rockfall deposits, (c) deposits of older (former) river terraces with rounded sediment of different grain size, and (d) deposits of the Mestiachala 2019 event. In Chapter 7 a simulation of the 2019 compound debris flow event in the Murkvami tributary was performed. It was aimed to back-calculate the 2019 event and thus to support the in-situ estimation of volumes released as a rock avalanche, of material deposited along the track as well as at the mouth of Mestiachala valley. The results are visualised in Attachment 8.

Geologically, the northern part of the investigated Mestiachala valley section is located in the massive crystalline rocks of Paleozoic age, the southern part in Jurassic slate geology (see Attachment 1). The Main Caucasus Thrust crosses rather perpendicular to the Mestiachala, exactly in the junction area with the tributary. The valley itself follows a major fault zone with probable lateral displacement of rock units (strike-slip fault). Especially the high and steep crystalline rock formations in the northwestern valley catchment form a large and voluminous release zone for rockfalls of different size. The southeast side is covered by deposits of rockfall from different grain sizes, however, these are in general to be considered as inactive as they are covered by shrubs and trees. Exceptions are bound to gullies feeding from the adjacent hillslopes, those are also pathways of snow avalanches if they are covered by grassland and Alnus type of vegetation.

Within the Mestiachala valley all current structures and potential new locations of the HPP1 are located, such as “Intake 1”, “Powerhouse”, “Gallery”, “Penstock” and the provisional “New intake”. For this reason, a detailed assessment of all hazardous locations is highly recommended. In the following, the assessment of geomorphology and related hazards is described clockwise from south to north on the orographic right side and from north to south on the left side. Additionally, geomorphological maps and geohazard maps are attached (Attachment 4, Attachment 6 and Attachment 7). Furthermore, In Chapter 7 a back calculation of the 2019 event as well as a model of a hypothetical debris flow in the Mestiachala valley were performed.

4.2 Mass movement inventory

4.2.1 Rockfall

Considerable rockfall areas are found mainly in the northwestern section along the gallery and northwards, where we have done additional studies (see 4.3 and 8.1). In the following chapter,

all potential detachments, independent from current degree of activity, will be assessed and described.

The first section in the Mestiachala valley endangered by rockfalls is the area on the foot of the large debris cone between the Mestiachala and Chalaati valleys (M-D1, Fig. 4-1). The release area of rocks and boulders can be localized about 700 m to 1,000 m above the power house below the peak of Mt. Dalrakora (M-R1). The release area is classified with a low to medium event frequency (see Attachment 6), the deposition area is a well forested debris apron and serves as rockfall protection.

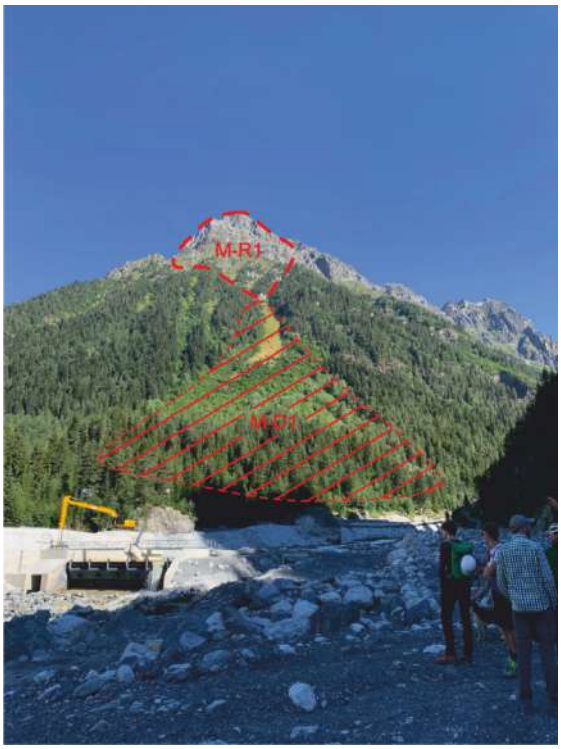

Fig. 4-1: Debris talus between Mestiachala and Chalaati valley with deposition and release area (M-D1, M-R1).

Close to the gallery four main deposition areas are located. In the area of M-D2 and M-D3 mainly very small rockfalls (<< 1 m³) but with a high frequency up to several events per year (EF 3 and 4) are expected. Only area M-R3a was identified as a clear and significant release area for these kind of magnitudes. A second possible release area with vertical rock towers is located about 450 m above the gallery (M-R3b, E316,570, N4,776,665). Expected magnitudes range between 2,500 m³ and 12,000 m³ ("Group 2 events" cannot be ruled out). So far, material is deposited behind the gallery, however, individual particles if following distinct parabolic saltation are expected to directly hit the roof and potentially destroy the structure. Detailed information is presented in Chapter 8.2.2. A visual overview of the locations can be found in Fig. 4-2 to Fig. 4-6.

Around 20 to 80 m northward the gallery the road crosses an area of high rockfall activity (shale) (M-R4, M-D4, Fig. 4-7), according to the observable high frequency (ranging from EF 2.2 to EF 4)

and considerable block sizes (see Chapter 4.3.2) the road is expected to be hit. A detailed rockfall simulation at this position was performed and will be discussed in Chapter 8.1.3. As a result respective protection is recommended (see Chapter 8.1.3 and 12.1.1).

Fig. 4-2: Deposition areas M-D2, M-D3, M-D4 and M-D5a adjacent to the gallery, view to the north.

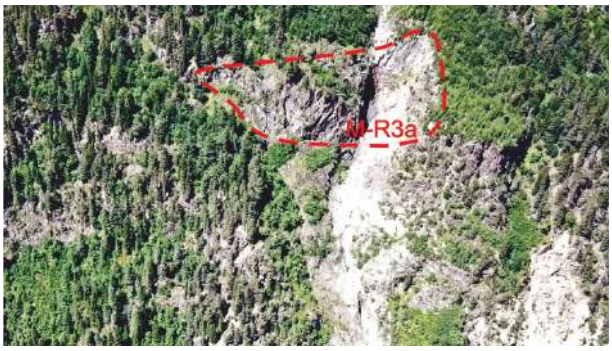

Fig. 4-3: Release area M-R3a along the gully, view to the west.

Fig. 4-4: Rock towers at release area M-R3b with volumes up to 12,000 m³. View to the SW.

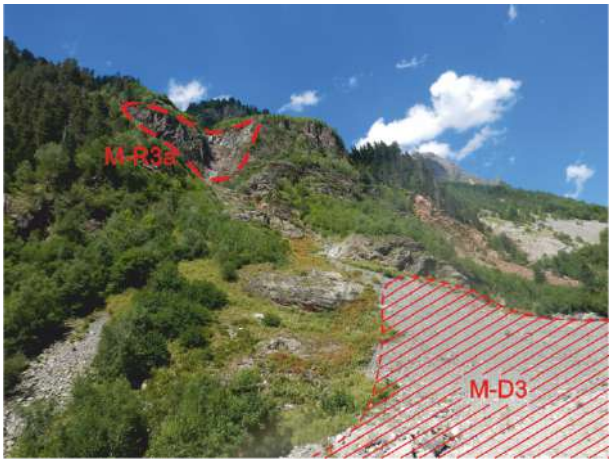

Fig. 4-5: Release and deposition area M-R3a and M-D3. View to the north.

Fig. 4-6: Detail figure of the release area M-R3a. View from below.

Fig. 4-7: Release and deposition area M-R4 and M-D4. View to the northwest.

From around 100 m northward of the gallery evidence for rockfalls with a magnitude < 5 m³ and an occurrence probability of 1-10 years and higher (EF 2.2 to EF3) was found (M-D5). In parts with a lower vegetation density and therefore lower protective effect (about 100 m to 200 m north of the gallery) some of the trajectories of falling blocks are expected to reach the road and river bed (M-D5a, Fig. 4-11).

Further northward, rockfall deposition is episodically taking place, and particle sizes can be considerable large (2 m in diameter and above), however, evidence was found that these events are expected to be in a range of 1-30 years (EF 2), and vegetation so far is expected to protect the respective road trench. The main release area linked to these deposition areas is located about 400 m to 700 m above the road (M-R5b, Fig. 4-8 and Fig. 4-9). There are also several hints of a single or several larger rockfall events originating from a notch close to the peak of Mt. Dalrakora about 1,300 m above the valley (M-R5a, Fig. 4-10).

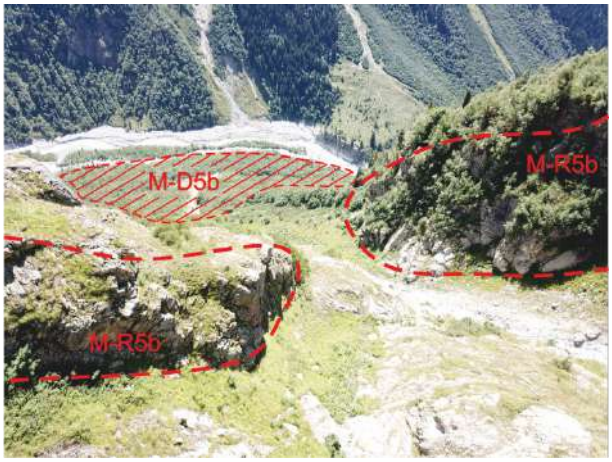

Fig. 4-8: Part of release area M-R5b, transit and deposition area M-D5. View to the southeast.

Fig. 4-9: Release area M-R5b. View to the northeast.

Fig. 4-10: Notch of release area M-R5a and on the left mountain ridge peak of Mt. Dalrakora. View to the northwest.

Fig. 4-11: Cut slope of construction road within the debris cone of deposition area M-D5a. View to the southwest.

Evidence for considerable rockfall activity (EF 2.2 to EF 3, see also Chapter 4.3) can also be found in the area north of the deposition of the 2019 event (M-D6, Fig. 4-12 to Fig. 4-14). Individual blocks are of a size of 4 m in diameter and beyond, these can reach the opposite river bank and may therefore be a hazard to the planned new intake. This may be taken into account when looking for an appropriate position for the new intake 1 structure. A detailed rockfall simulation was performed. The results are presented in Chapter 8.1.4. Depending on the final position of the new intake 1 respective technical protection is recommended (see also Chapter 10.1.2 and 12 for detailed information). Minor gullies are also subject to hillslope debris flow accumulating on the rockfall deposition and/or reworking it.

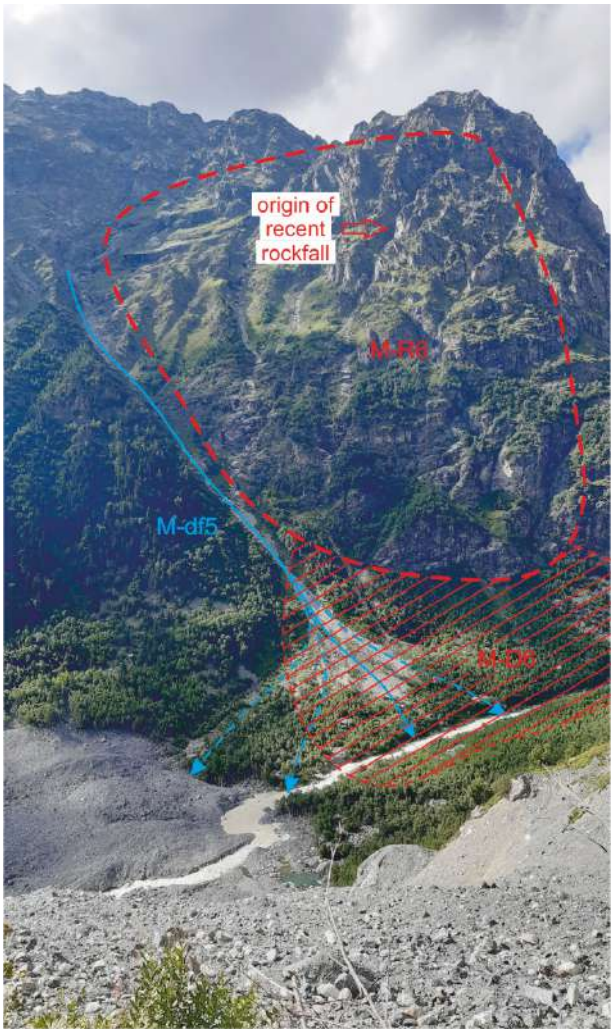

Fig. 4-12: Debris flow channel (M-df5), release area (M-R6) and deposition area (M-D6) north of the 2019 event deposits and opposite of the location of the new intake. View to the northwest.

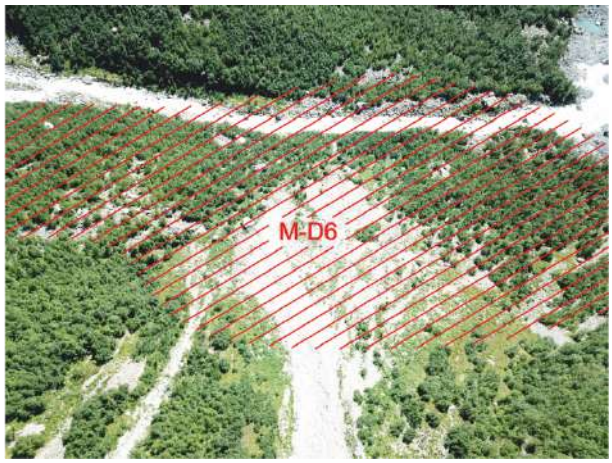

Fig. 4-13: Deposition area M-D6. View from above to the east.

Fig. 4-14: Deposition area M-D6, view towards the debris flow channel (M-df5) from below. View to the west.

On the opposite side of the valley (orographic left) and north of the tributary valley several areas with a high relief and steep rock faces are located that are possible release areas for future rockfall of different magnitude (M-R7, Fig. 4-15).

Furthermore a notch with a length of about 280 m and a more or less vertical northern rockface of about 30 m to 50 m height is located a few hundred meters to the south (Fig. 4-16 and Fig. 4-17). This notch is interpreted as a release or detachment area of a past rockfall or rockslide event (M-R8).

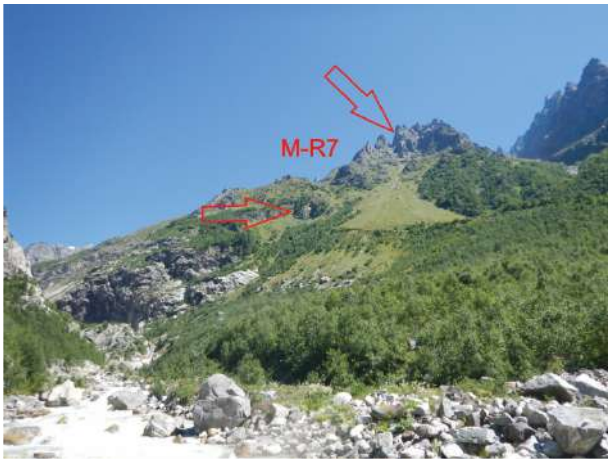

Fig. 4-15: Release area M-R7, view to the northeast.

Fig. 4-17: Release area M-R8, view to the northeast.

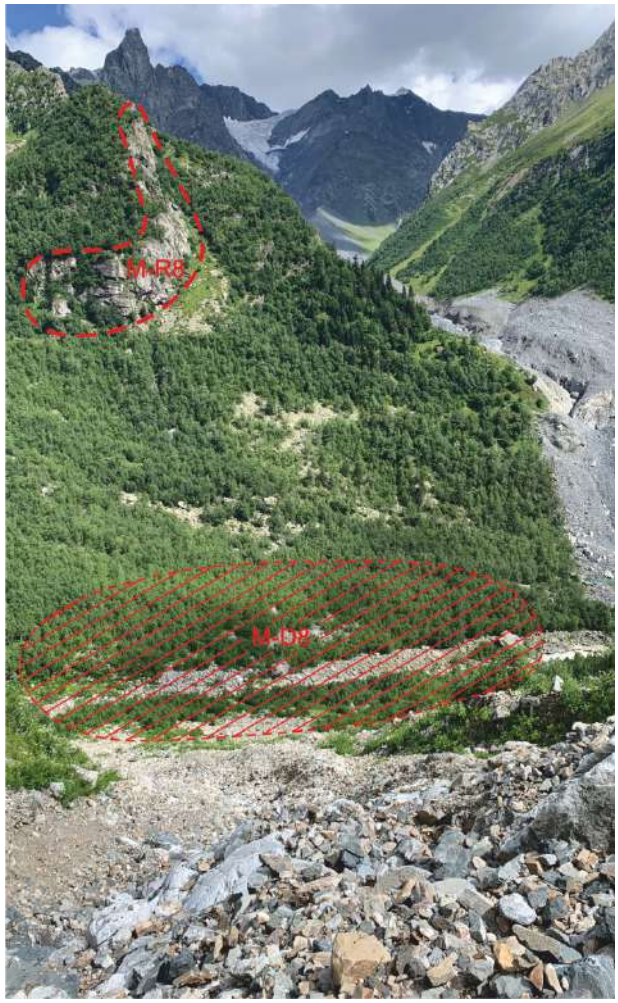

Fig. 4-16: Release and deposition area M-R8 and M-D8, view to the east.

On the orographic left of Mestiachala river and east of the power house there are also indications of possible future rockfalls (M-R9) in the steep mountain ridge (Fig. 4-18). First estimations show magnitudes of several cubic meters to hundreds of cubic meters.

Fig. 4-18: Possible release and deposition area M-R9 and M-D9, view to the east.

4.2.2 Debris flow

All rockfall deposition areas with gullies in the transit areas are characterized by debris flows as secondary processes shaping the cone surfaces. Those areas directly adjacent to the gallery up to the old desander (sedimentation basin) (M-df2 to M-df4, M-df5) and the area north of the power house (M-df1) are shown in Fig. 4-19, however, these are only of minor importance for delivering considerable amounts of material to the valley bottom and consequently to the Mestiachala river. Hence, even if activity is rated as high, effects are negligible.

Attention has to be given to the debris flow channel depositing material behind the 1850 lateral moraine at the left side of Mestiachala at E318,480, N4,777,555 (M-df6, Fig. 4-20) as debris flow run out is trapped behind the moraine at a length of 180 m and possible further deposition volume is limited. In case of future events overtopping the moraine crest, considerable incision will result and 10,000 m³ of unconsolidated material (of morainic origin and debris flow material) is expected to be deposited in the river channel as well as in the area foreseen for building the new intake 1. Major source areas are located at the upper northern part of the catchment in unconsolidated gullies and lateral glacial moraines at 3,000-3,200 m asl, however, so far these were not released with considerable volumes and transported downhill. Consequently, frequencies and magnitudes cannot be quantified, potential magnitudes, however, are expected to be several thousands of m³. Hence, with a distinct uncertainty a major hazard has to be expected for the area foreseen for the new intake 1 as well as for the entire Mestiachala river channel.

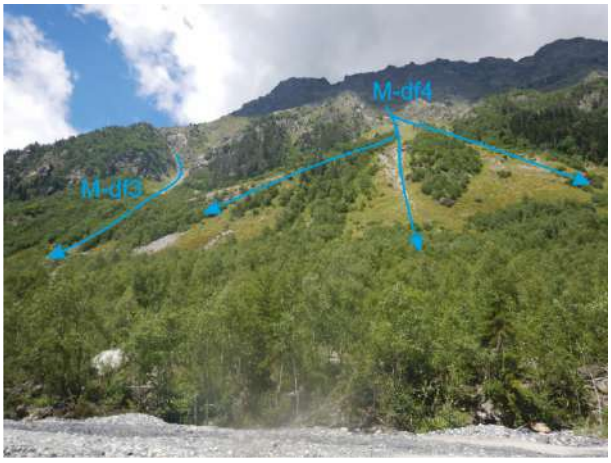

Fig. 4-19: Transit areas of old rockfall cones with debris flows as secondary processes. Here M-df3 and M-df4. View to the west.

Fig. 4-20: Debris flow M-df6 coming from a catchment north of Murkvami valley. Deposits were trapped behind the moraine. View to the east.

With respect to possible future debris flow-like events originating from the Tributary, please see our comments in Chapter 3 and the simulation results in Chapter 7 and Attachment 8. Generally, an event such as the 2019 event may again occur in the future, however, for such large events possible frequencies and magnitudes can only be given based on scenario interpretation.

Further minor debris flow deposition areas are located on the cones along the southeastern (left) valley flanks, usually in association with snow avalanche run-out areas (M-df7 to M-df9, Fig. 4-21 and Fig. 4-22). Magnitudes are of minor importance (several 100 m³ maximum) for delivering sediment to the Mestiachala river, and frequencies were assessed with 1-30 years (EF 2) and beyond, depending on the meteorological conditions.

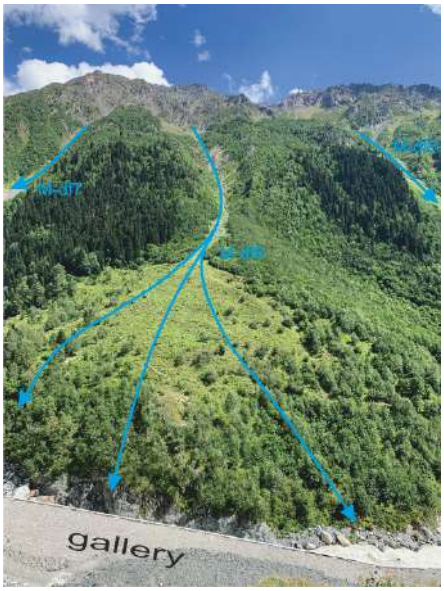

Fig. 4-21: Debris flow channel M-df8 on the opposite of the gallery. View to the south.

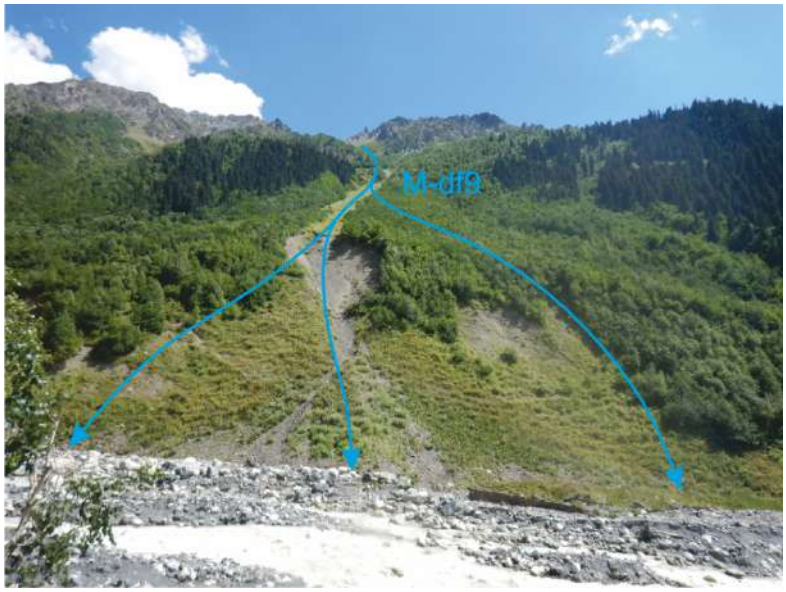

Fig. 4-22: Debris flow channel M-df9. View to the east.

4.2.3 Channel bed

The channel bed of Mestiachala river has been incised around 5 m since the 2019 event (13 months), and distinct river terraces of up to 2 m height have been developed in particular in the middle reaches of the evaluated trench on the left side. The material of these terraces is composed of a mixture between the original granitic material (in-situ and transported from the Lekhziri catchment in the north) and deposits from the Tributary, and may be eroded during future periods of high discharge. It is evident that the discharge and water level of the river is highly variable during daytime as well as over the year, examples include the waterless channel directly adjacent to the main river channel crossing the 2019 deposits; this channel will be filled up only if water level in the river is raising around one meter above the currently observed water level and will continuously erode the available deposits from the 2019 event. These fluctuations are supplemented by possible extraordinary events such as those originating from the outbreak of subglacial water pockets (evidence for such episodic events was found along both of the Lekhziri glaciers during analysis of the Pleiades imagery (see also Chapter 9)) as well as from possible breaking-up of the dead ice located in the front part of the valley (as the August 2018 event, see Fig. 4-23 and Fig. 4-24). Magnitudes and frequencies, however, may not be provided with reliable accuracy at the present stage. A simulation of a high magnitude debris flow was performed. The results are presented and discussed in Chapter 7.4 as well as in Attachment 8.

The bottleneck for lateral channel erosion is located 80-110 m northward the gallery in the sharp left turn of the river channel. Erosion continuously takes place, and will be increased in case of high discharge. Mitigation is required to protect the road as well as the pipe (see Chapter.12.1.3).

Fig. 4-23: Dead ice in the lower Lekhziri catchment prone to remobilisation in case of high discharge. View to the south.

Fig. 4-24: Dead ice in the lower Lekhziri catchment prone to remobilisation in case of high discharge. View to the north.

4.3 Input data for rockfall simulations in specific hazard areas

During the field campaign, rockfall data were assessed (block sizes, structures of detachments, activity, damping factors, roughness of transit and accumulation areas,…). These are essential to undertake the required simulations for an assessment of the hazard for the penstock pipe and the potential new intake structure. The rockfall simulations are necessary to determine the design values for impacting energy and bouncing height and for determining an optimized location for protection measures in the fall trajectory. Rockfall simulations in Chapter 8.1 were performed only at locations that are prone to high-frequency rockfall events such as the gallery or the construction road (M-D4) and the estimated position of the new intake 1 (M-D6). Based on the simulation results, rockfall protection measures to protect the HPP infrastructure from frequent but individual rockfall events will be suggested (Chapter 12.1).

The modelling and data acquisition strictly follows the Austrian Standard ONR 24810 “Technical protection against rockfall”.

4.3.1 Rockfall hazard zones

Areas prone to rockfall deposition pose an imminent threat to the HPP infrastructure and the operating staff, and have been identified in the Mestiachala valley along the section of the avalanche gallery. In particular, these areas include location M-D4 above and north of the gallery. Other areas affected by frequent rockfall events are M-D6 located close to the potential new intake location. These two locations along the gallery and at the new intake location show evidence for frequent rockfall activity, as proxied by recently deposited boulders, impact marks on the land surface and on trees, as well as detachment areas having been observed above these locations. Based on these observations and the data collected during the previous site visits in 2018 and 2019 it has to be concluded that minor and medium rockfall (< 5 m³ up to 10 m³) occurs frequently in these areas. A frequency of up to ten events per year resulted in the event frequency classification EF3 according to ONR24810.

In addition to these frequently occurring rockfalls we would like to highlight observations made at locations M-R3b and M-R5b situated several hundred meters above the valley bottom and showing three instable rock towers with estimated volumes of several thousand cubic meters. These towers show signs of instability and displacement, leading to an event frequency class EF2 rating (1 event within 1-30 years) for large events with up to 10,000 m³ or even very large events (> 10,000 m³). Furthermore, location M-R8 on the orographic left side of the river and close to the estimated position of the new intake 1 is interpreted as a release area of a past rock slide event. During the field investigations no evidence for relevant rockfall deposits originating from M-R8 was found in the area around the estimated new intake 1 position. We presume released rocks will disintegrate when moving downhill and will be deposited along the overgrown slope.

However, depending on the block size a low-frequency but high-magnitude event will be accumulated at the position of the new intake 1.

4.3.2 Characteristic rockfall block sizes

In order to determine the design block for rockfall modelling of frequently occurring rockfall events, block measurement of axes from randomly selected blocks in the deposition areas M-D4 and M-D6 as undertaken and a statistical distribution of block sizes has been computed. The characteristic design block size V97 (97 % of blocks have a volume equal to or less than V97) is obtained as a fractile value of the block size distribution and corresponds to the event frequency class EF3. As a result, the design block for a rockfall simulation for M-D4 was determined with **5.40 m³** and for M-D6 with **8.50 m³.**

Fig. 4-25: Examples of comparably fresh rock blocks in M-D6.

Fig. 4-26: Examples of fresh rock blocks in M-D4.

4.3.3 Conclusion on rockfall hazard

Detailed results of the rockfall simulation in the areas M-D4 and M-D6 are presented in Chapter 8.1. Nevertheless, based on the determined design block size and the evidence for impacts recorded close to the buried penstock pipe, **the rockfall hazard in the above-mentioned areas has to be classified as "high"**. Furthermore, the need for locally applied rockfall protection measures is very likely for these highly-frequent rockfall events.

However, less-frequent but high-magnitude events will still pose a threat to elements at risk. These include possible events released at the instable rock towers (e.g. M-R3b); for those events it is currently not possible to predict release time, exact magnitudes and mechanical behaviour of the rock masses (see Chapter 8.2.2).

5 Recorded situation of Chalaati valley

5.1 General data

Chalaati valley is a right tributary of Mestiachala valley, spanning from 1,646 m asl (HPP 1) to 4,412 m asl (Chatintau) and the North and South Ushba, 4,698 and 4,700 m asl, points of highest elevation. The valley is covered by two glacier tongues confluencing in the middle part of the valley at 2,350 m asl, one reaching north towards Bzhedukh peak (4,280 m asl) and the other towards Chalaati pass (4,120 m asl). The current glacier mouth is located at 1,880 m asl with the lower part of the glacier being covered by considerable amounts of debris and rockfall deposits from the adjacent valley margins. Currently, the glacier is retreating with an annual average of 12 - 15 m (see also Chapter 9). The mean channel gradient between the HPP 1 and the glacier mouth is 6.5° (11.5%).

Geologically, the southern part of the Chalaati valley is located in the Jurassic slate geology. The Main Caucasus Thrust with massive crystalline rocks of various origin and type crosses in oblique angle few tens of meters north of the current glacier mouth (see Attachment 1).

The entire valley is characterized by steep lateral topography and corresponding high elevation differences. The valley bottom is covered by deposits originating from (a) unconsolidated ground moraine material of different geologic origin, (b) end moraines of different glacier retreat states and (c) deposits of multiple types of mass movements. The valley shows a typical succession of vegetation cover of different species, depending on the micro-climatic condition and the glacier retreat. Moreover, the valley bottom is covered by large amounts of re-mobilised and deposited gravel of different grain sizes which are sporadically transported by Chalaati river downwards the valley, depending on the highly-variable discharge volume. Discharge volume was not further quantified, and records are missing because of missing gauging stations in the catchment. Further information on possible discharge volumes is available in the Hydroconsult reports of February 2015, April 2016 and November 2019, with an approximated 1/10 discharge volume of 42.4 m^3/s, and a 1/30 discharge volume of 57.3 m^3/s.

The detailed results of field investigations and event analysis, distinguishing rockfall and flow processes over the entire study area along the Chalaati valley are described in the following Chapters. Additionally, geomorphological maps and geohazard maps are attached (Attachment 3, Attachment 6 and Attachment 7).

5.2 Mass movement inventory

5.2.1 Rockfall

The entire northeast-facing valley flank is influenced by mass movements of rockfall type originating in the bedrock cliffs and developing large cones and deposition areas alongside the valley margin, associated with rockfall from loose material originating in the 1850 lateral moraine. Grain sizes are highly variable, depending on the underlying geology and state of weathering. Going from the valley mouth towards the valley head, the following sites are of relevance for HPP1.

At E316,000, N4,775,500 a rockfall area is located with the left (eastern) part (C-R1a) being more active than the right (western) part (C-R1b). The overall dimension is approx. 195 m in length and 100 m width (Fig. 5-1 and Fig. 5-2). Block sizes include particles of 10 m and below. From the left part, individual blocks may reach the Chalaati river channel bed (C-D1), but with no significant influence on sediment availability for the water body. Parts from the bedrock cliff on the left side may be even highly active but do not deliver considerable volumes to the channel.

Adjacent valley margins (C-D2) are covered by deposition of inactive rockslides with different block sizes over a length of 630 m with no significant relevance in terms of material provision for channel erosion. The release areas C-R2 are to be found in the steep to vertical rockfaces along the valley flank (Fig. 5-3).

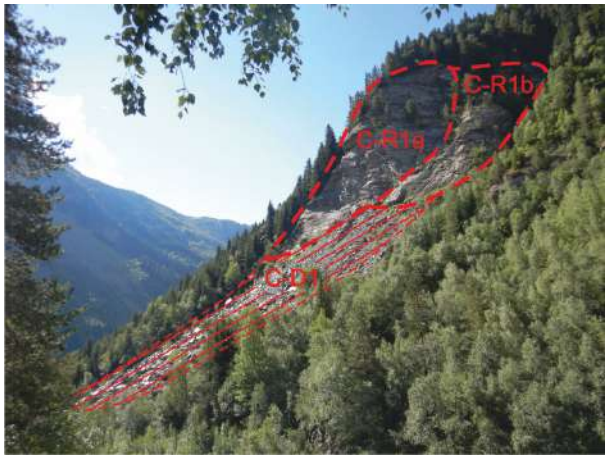

Fig. 5-1: Release areas C-R1a, C-R1b and part of the deposition area C-D1. View to the southeast.

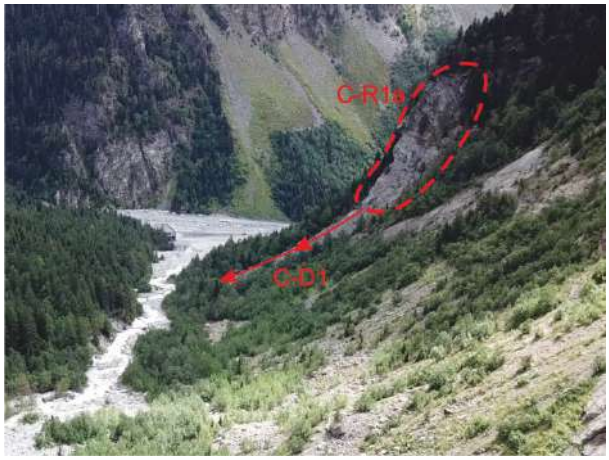

Fig. 5-2: Release area C-R1a and part of the deposition area C-D1. View to the southeast.

Fig. 5-3: Eastern part of area C-R2. View to the south.

At E315,200, N4,775,800 two distinctive deposition cones are located (C-D3), both composed from phyllite material (C-R3) showing similar smaller block sizes and not providing significant amounts of material to the channel (Fig. 5-4 and Fig. 5-5).

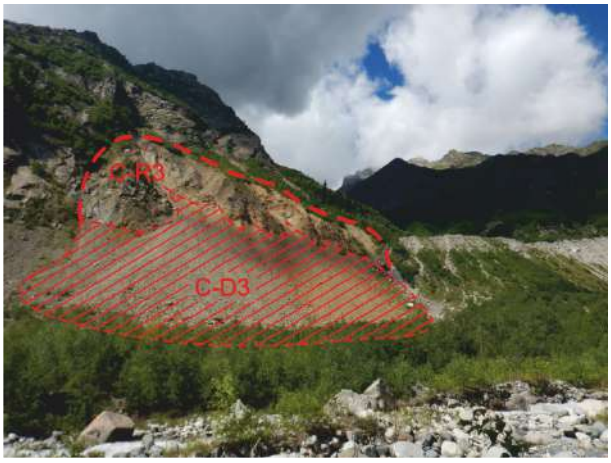

Fig. 5-4: Release and deposition area C-R3/C-D3 (reddish area) as well as area of debris flows C-df3. View to the southwest.

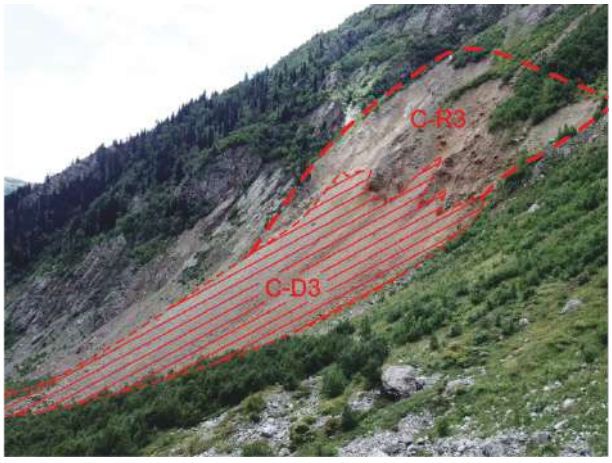

Fig. 5-5: Release and deposition area C-R3/C-D3 (reddish area). View to the southeast.

The adjacent 1850 moraine with a length of 475 m provides material (C-R4) which is transported downslope as rockfall with block sizes up to approx. 10 m in diameter, these may reach the channel and opposite valley bottom (C-D4, Fig. 5-6). Overall, rockfall is active but does not provide significant material to the channel because of sporadic release of individual blocks.

Further inwards, a more active zone of phyllite material and smaller grain sizes is located (C-R5) and material is deposited from the bedrock above (E314,820, N4,776,330) (C-D5, Fig. 5-7). Parts of the blocks are also deposited on the orographic left side of the current channel bed. Occurrence probability is 1-10 years and magnitude is small.

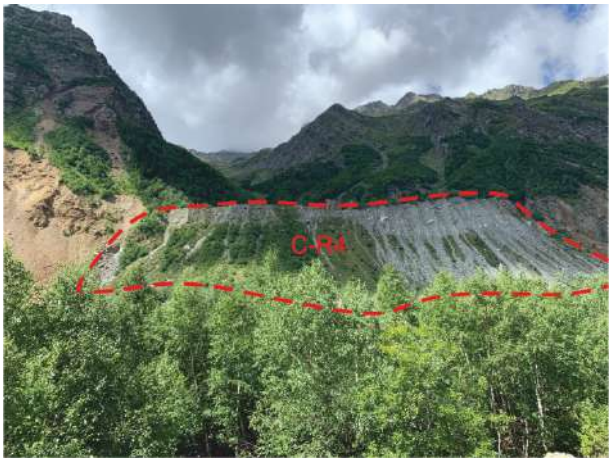

Fig. 5-6: Release and deposition area C-R4/C-D4 at the 1850 moraine on the southwestern valley flank. View to the southwest.

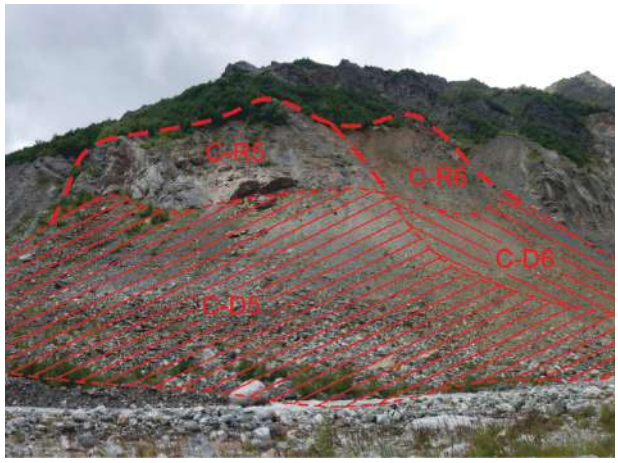

Fig. 5-7: Release and deposition areas C-R5/C-D5 (left) and C-R6/C-D6 (right). View to the southwest.

Adjacent, bedrock composed from shale with large boulders up to 12 m is released (C-R6) and deposited in the valley bottom on both sides of the channel bed (C-D6), activity is 1-10 years and higher (EF 3) and magnitudes may be considerable during repeated events, these may even be more frequent during thunderstorms and heavy rainfall periods. Material is highly fragmented and smaller grain sizes are highly prone to mobilization during episodes of high discharge of Chalaati river. This may have considerable potential for subsequent sediment transport and debris flow in the river down to HPP1, even if the channel gradient is comparably low.

Further inwards, bedrock composed from quartzite releases large boulders (up to 20 m and above; C-R7) currently deposited at the lower part of the glacier tongue (E314,540, N4,776,650) (C-D7) but highly prone to mobilization due to the glacier retreat (Fig. 5-8). As such, parts of the deposition already can be found in the glacier forefield and along the river channel/glacier mouth. Activity is very high with several events per year (EF3-4) and deposition provides considerable hazard to HPP1 in conditions of high discharge or the possible outbreak of sub-glacial water pockets.

Fig. 5-8: Release area C-R7, in the front the glacier mouth. View to the west.

Finally, additional rockfall areas are located lateral to the glacier tongue (C-R8) and deposit material on the ice body (C-D8). This material may become available once glacier retreat is continuing. Currently, glacier retreat rates are approx. 12 - 15 m per year (Fig. 5-9 and Fig. 5-10).

Along the southwest-facing valley flank, rockfall areas are mostly associated with the 1850 lateral moraine (C-R9), deposition occasionally may reach the channel bed (C-D9a, Fig. 5-11 and Fig. 5-12). Individual large boulders with 2 - 3 m diameter endanger the trail episodically, two of these boulders can be found at E315,630, N4,775,840 (C-D9b).

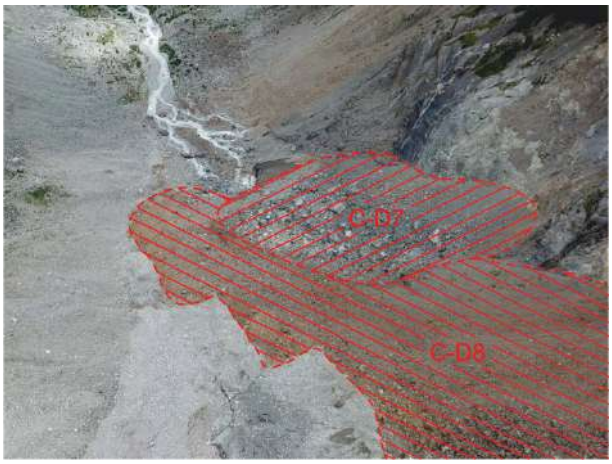

Fig. 5-9: Deposition areas C-D7 and C-D8 on the glacier tongue: C-D7 in the back includes big greyish boulders and C-D8 in the front with smaller reddish rocks; the rockfall material is constantly transported by glacier movements. View from above to the southeast.

Fig. 5-10: Release area C-R8 and deposition area on top of the glacier tongue C-D8. View to the southwest.

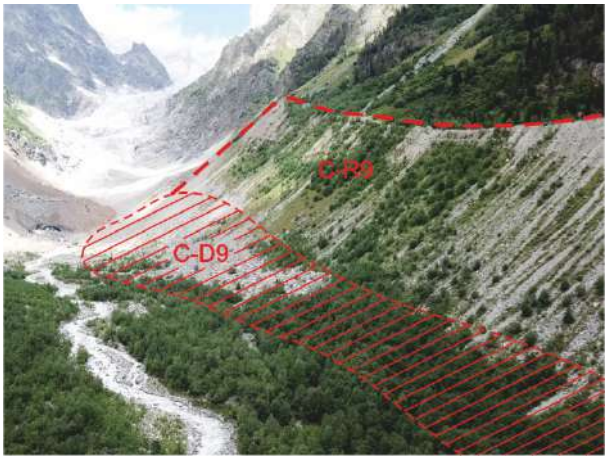

Fig. 5-11: Western part of the moraine and the release and deposition area C-R9/C-D9. View to the north.

Fig. 5-12: Southeastern and upper part of the release area C-R9, some larger and exposed boulders are located close to the crest. View to northeast.

Fig. 5-13: Frequent fresh rockfalls hitting on hiking path, detached from release area C-R9.

5.2.2 Debris flow

Along the northeast-facing lateral valley flank, a number of smaller debris flows (hillslope type) are detectable on the deposits of the rockfall areas. Affected cones are located at E315,830, N4,775,600 (C-df1, Fig. 5-14) with dimensions of 65 m width and 50 m length, and at E315,570, N4,775,530 (C-df2, Fig. 5-15) with three smaller deposits associated with respective release areas in locally weak layers of the bedrock. Further surficial (secondary) debris flow processes are associated with the rockfall cones at E315,200, N4,775,800 (C-df3), at least three different deposits can be distinguished with a total extent of approx. 200 m width and 200 m length. All these debris flows only deliver minor magnitudes that do not reach the river channel. However, they occur on a regular basis as a result of mass wasting on these rockfall cones. Similarly, the 1850 lateral moraine (C-df4) is reworked by surficial hillslope debris flows of minor magnitudes with deposition on the valley margin not affecting the river channel during normal discharge conditions as these are located on an older river terrace.

Fig. 5-14: Area of debris flow C-df1, view to the southwest.

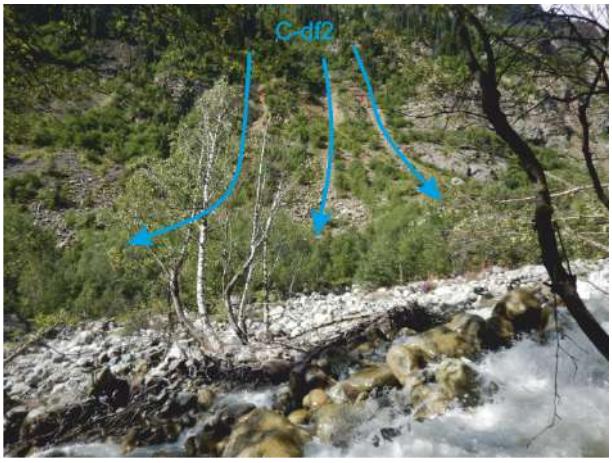

Fig. 5-15: Area of debris flows C-df2. View to the southwest.

The southwest-facing valley flank shows some inactive old debris flow deposits of considerable magnitudes (10,000 m³), however, these are not relevant with respect of delivering material to the river channel as they are located on a higher (older) river terrace. Most of these are of an age of 50 - 100 years. A potentially larger event may occur at E315,220, N4,776,280 (C-df5, Fig. 5-16) where currently only a minor deposit is traceable (50 m width, 100 m length), however, the release and transit area is characterized by a considerable amount of loose material and considerable gully erosion is detectable. Frequencies are assessed with active (11 - 30 years).

Fig. 5-16: debris flow channel C-df5 on top of the moraine crest. View to the northeast.

The largest debris flow deposit is located northeast of the current glacier mouth directly adjacent to the glacial deposits and the glacier body (Fig. 5-18 and Fig. 5-17). The fan apex is located at

E314,660, N4,777,250 (C-df6) and a series of different large depositions can be found below with a slight orientation downwards the overall inclination. Older deposits are of approx. 230 m width and 600 m length, with varying height and an approximated volume of 400,000 m - 700,000 m³. Sediment sizes are highly variable and reach from sand and silt fraction to boulders with a diameter of 1 m - 2 m and singular boulders with larger volume. Younger deposits vary between approx. 10 m and 20 m and a length of 100 m to 200 m with similar heights (1,000 - 100,000 m³).

Fig. 5-17: Debris flow channel C-df6 with a high amount of sediment, view from above to the northeast.

Fig. 5-18: Debris flow area C-df6 with the channel on the right and the deposition area on top of the glacier tongue, view from above to the southeast.

The deposited volumes may become mobilized if the glacier tongue retreat is reaching this area. Moreover mobilization may also occur if subglacial water bodies break out and discharge lateral of the glacier body, however evidence for such processes was not found during the field work. Furthermore potential future debris flows from the same release area may remobilize the deposited material towards the channel bed, presumably together with parts of the glacier tongue. Remobilization of deposited rockfall masses (see above) is highly probable. These masses may then travel further down the Chalaati valley to HPP1. Magnitudes may be comparable to the 2019 Mestia event, potential frequency, however, remains open.

6 Electrical resistivity tomography and interpretation

Geophysical methods have been applied in geotechnical studies for a considerable period. By contrast to direct exploration e.g. via drilling, the general principle of geophysical exploration is to collect data uninfluential over long distances. In the Mestiachala valley the geoelectrical method of “Electrical Resistivity Tomography” (ERT) was applied in a two-dimensional manner giving linear results along a transect.

6.1 Scope of investigation

Results of the ERT measurements should provide below listed information to gain a better understanding of the geological conditions being used for modelling of future compound process events.

The July 2019 event was a compound process resulting in a cascade of different types of mass movements. To adequately reflect this event, its processes and behaviour in a model (Chapter 7), one of the most important input data is the overall volume of the failed rock mass. A first rough estimation was done by performing a remote analysis of satellite imagery. To verify the resulting information on volume, two orthogonal transects (“Intake 1, SW-NE” and “Intake 1, SE-NW”) were carried out on top of the main deposition opposite the Tributary/Murkvami valley. In addition to the thickness of the event deposits, these transects furthermore provide information about the surface depth of the solid rock and insights about additional processes during the impact.

A second key question as an input parameter to debris flow modelling concerns the ability of an event to remobilize existing deposits along the runout. The solid rock surface depth and its topography along the runout path as well as the type of potentially remobilized sediments are required to gain a better understanding of the geological conditions and to verify the chosen model parameters. In order to confirm above, a third transect (“Mestiachala, gallery”) was performed along the Mestiachala valley.

6.2 Method of electrical resistivity tomography

6.2.1 Electrical resistivity and its influencing factors

According to Ohm’s law the electrical current in a conductive medium is direct proportional to the voltage. The specific electrical resistivity is considered in this equation as a constant of proportionality. The resistivity of a specific material depends on the ability to mobilize ions which in turn transport electrons. The water content of a material and the salinity of this pore water

are of major importance. Depending on the physical properties of the material (in this case the subsurface material) it can store more or less water., whereas its chemical properties additionally influence the chemical composition of the pore water. In contrast, air-filled pore space acts like an insulator. The following rock properties are most important in influencing the specific resistivity (SAMOUËLIAN et al. 2005).

Grain size distribution: As the grain size decreases, the specific surface of the material increases (e.g. clayey substrate has a very large specific surface). This means that more water will be capped back and the resistivity decreases.

Porosity and pore geometry: These properties determine the ratio between air and water in the substrate. In general porosity promotes water saturation (lower resistivities), but if it exceeds a certain level, the pore water content decreases and the pore space is filled with air (higher resistivities. The same effect can be caused by unfavourable geometry.

Connectivity: In case of a good connection between the pore spaces, complete water saturation is possible. Subsequently, the resistivity decreases.

Degree of fracturing: The degree of fracturing in solid rock formations and the percentage of fractures filled with groundwater versus air are highly relevant for the resistivities measured.

Salinity of the pore and fissure water: More or less ions are available to transport electrons depending on the origin of the pore water (rainfall, infiltration of river, lake or salt water, transport through different rock formations, etc.), the transport time through the aquifer and chemical properties of the aquifer material (e. g. minerality, possibility of solution weathering, etc.). Consequently, electrical resistivity de- or increases.

Temperature: As the temperature rises, the viscosity of a fluid (here pore water) decreases and thus the ion movement increases. The result is a lower resistivity.

Resistivities of various rocks and sediments are listed in Tab. 6-1. Solid rocks are typically characterized by high resistivities, whereby the resistivity here particularly depends on the degree of fracturing and the percentage of fractures filled with groundwater. As a result, these rock types can show a wide range of resistivity values.

Tab. 6-1: Resistivities of various rocks and sediments (Milsom 2003, Telford et al. 1990).

Rock material	Resistivity range [Ωm]
Surface/soil water, fresh groundwater	10 – 100
Topsoil	50 – 100
Clay	1 – 100
Loose Sand	500 – 1000
Gravel	100 – 600
Weathered bedrock	100 – 1000
Slate	500 – 500,000
Quartzite	500 – 800,000
Granite	200 – 100,000

6.2.2 Measurement setup and arrangement

Geoelectrical measurements are based on the difference in resistivity between different sub-surface materials. To determine the resistivity at a certain point, a potential is maintained via point (current) electrodes that causes a DC (direct current) flow through the ground. This potential is measured by two other (potential) electrodes which are geometrically arranged. Based on the measured values an apparent resistivity value is calculated.

In case of a one-dimensional (1-D) survey only four electrodes are in use. While the centre of the four electrodes remains constant only the current electrodes or both the current and potential electrodes (depending on the selected array) move stepwise to both sides. The wider the electrodes are apart, the deeper the electrical field penetrates the ground and a vertical profile under the approximate middle of the section is created (ETZELMÜLLER et al. 2003).

Creating a two-dimensional (2-D) profile the 1-D technique is further developed, using 60 electrodes or more at a time. A controller unit automatically switches between numerous electrode configurations. As shown in Fig. 6-1 each array of four electrodes has to be moved step by step over the measurement profile during the measurement series while each electrode will be used as both current (A and B) and potential electrode (M and N). With each step, a data point is generated exactly in the middle of the four electrodes. The penetration depth is varied by changing the distance between the electrodes. The maximum depth is approximately one sixth of the maximum (current) electrode spacing. By using suitable software (in this case Res2DInv-software) an inversion of the gathered data produces a 2-D section of the subsurface resistivity (SCHROTT et al. 2008).

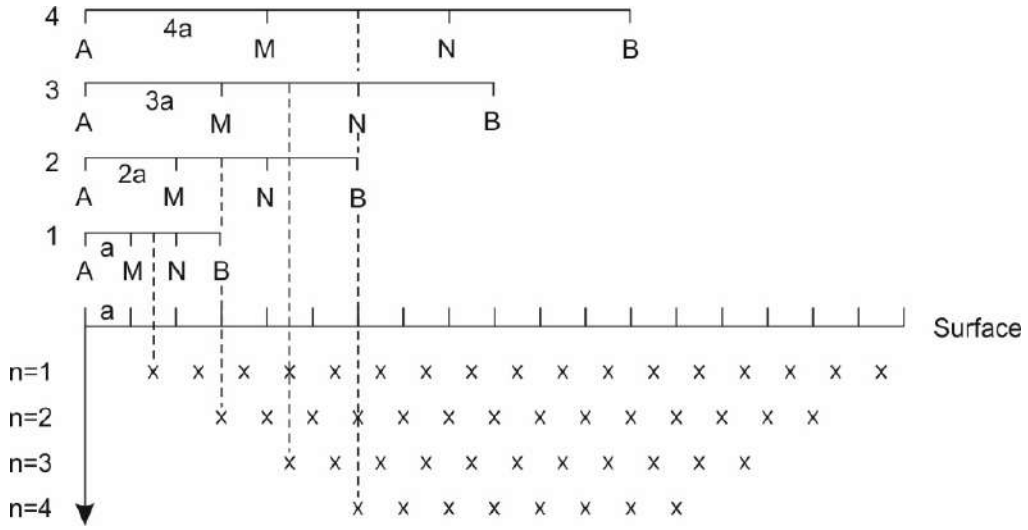

Fig. 6-1: Schematic sketch of the measuring arrangement of a "Wenner" array with a single electrode spacing a, current electrodes A and B and potential electrodes M and N. With increasing electrode spacing n = 1-4 the penetration depth of the data points increases. The horizontal position of the data points is always in the centre of the electrodes that are in use (modified after SAMOUËLIAN et al. 2005: 181, Fig. 4).

In geosciences different electrode arrays with different geometric factors exist. Each array can be used to answer different questions. The so called "Wenner" array (Fig. 6-2) shows a good signal - noise ratio and at the same time is favourable for the detection of horizontal layers and structures. It was therefore used in the present case.

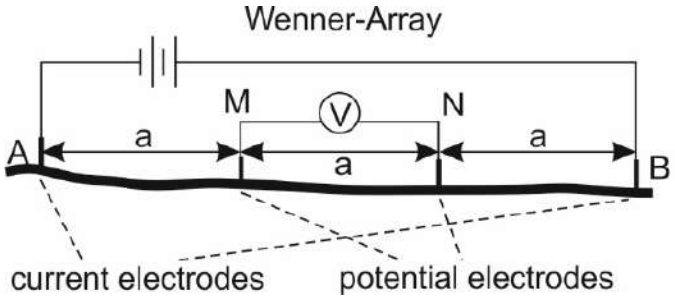

Fig. 6-2: Schematic arrangement of the "Wenner" array with current electrodes A and B, potential electrodes M and N and electrode spacings a (modified after HACK 2000: 440, Fig. 11).

In the Mestiachala valley, the device "ABEM Terrameter LS2 for resistivity and IP imaging" with four cables (length of each cable 100 m) and 81 electrodes (maximum electrode distance of 5 m) was used. This arrangement allows a 400 m long measurement to be carried out. If an even longer transect is needed a so-called "roll-along" method has to be applied. After a first measurement with only three cables and a second with all four cables, the first cable will be unplugged and installed again at the end of the last cable (Fig. 6-3). Proceeding in this way an endless transect could be possible.

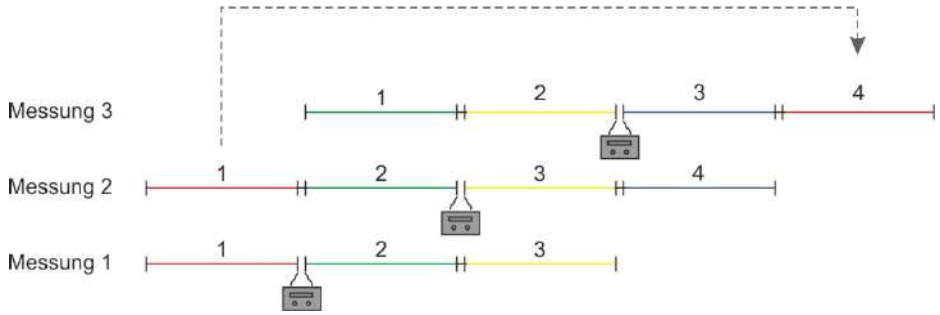

Fig. 6-3: Schematic sketch of a "roll-along" measurement.

6.3 Results of ERT in Mestiachala valley

6.3.1 Data collection

During the field trip in August 2020 three geoelectrical transects with lengths of 300 m, 500 m and 700 m were performed in the Mestiachala valley. The location of the transects and the results after the inversion process are displayed in Attachment 9 and can also be found in figure Fig. 6-5 and Fig. 6-6. Tab. 6-2 shows the basic information of the three geoelectrical transects.

Tab. 6-2: Geoelectrical transects in the Mestiachala valley

ID	Coordinates (UTM zone 38T)		Minimum electrode spacing (a) [m]	Transect length [m]	Transect max. depth [m]	Number of data points
	Start east / north [m]	End east / north [m]				
Mestiachala, gallery	316,551 / 4,775,792	319,972 / 4,776,323	5	ca. 700	ca. 65.6	786
Intake 1, SW-NE	317,630 / 4,776,905	317,905 / 4,777,311	5	ca. 500	ca. 60.8	561
Intake 1, NE-SW	317,897 / 4,777,078	317,680 / 4,777,250	5	ca. 300	ca. 47.8	210

6.3.2 Data processing

Editing the data (e. g. elimination of bad datum points) and the inversion process was done by using the Res2Dinv-software. As described in Chapter 2.2 the geological conditions in the Mestiachala valley are expected to be highly inhomogeneous (e. g. valley sediments differing in genesis of deposition and therefore in petrographic composition and granularity, solid rock with a rough topography underlying the sediments). These inhomogeneous conditions lead to noisy data. Therefore, the setting "robust inversion" was chosen for all three transects. By defining a robust constraint, the inversion is less sensitive to very noisy data points but might give a higher apparent resistivity RMS (root-mean-square) error.

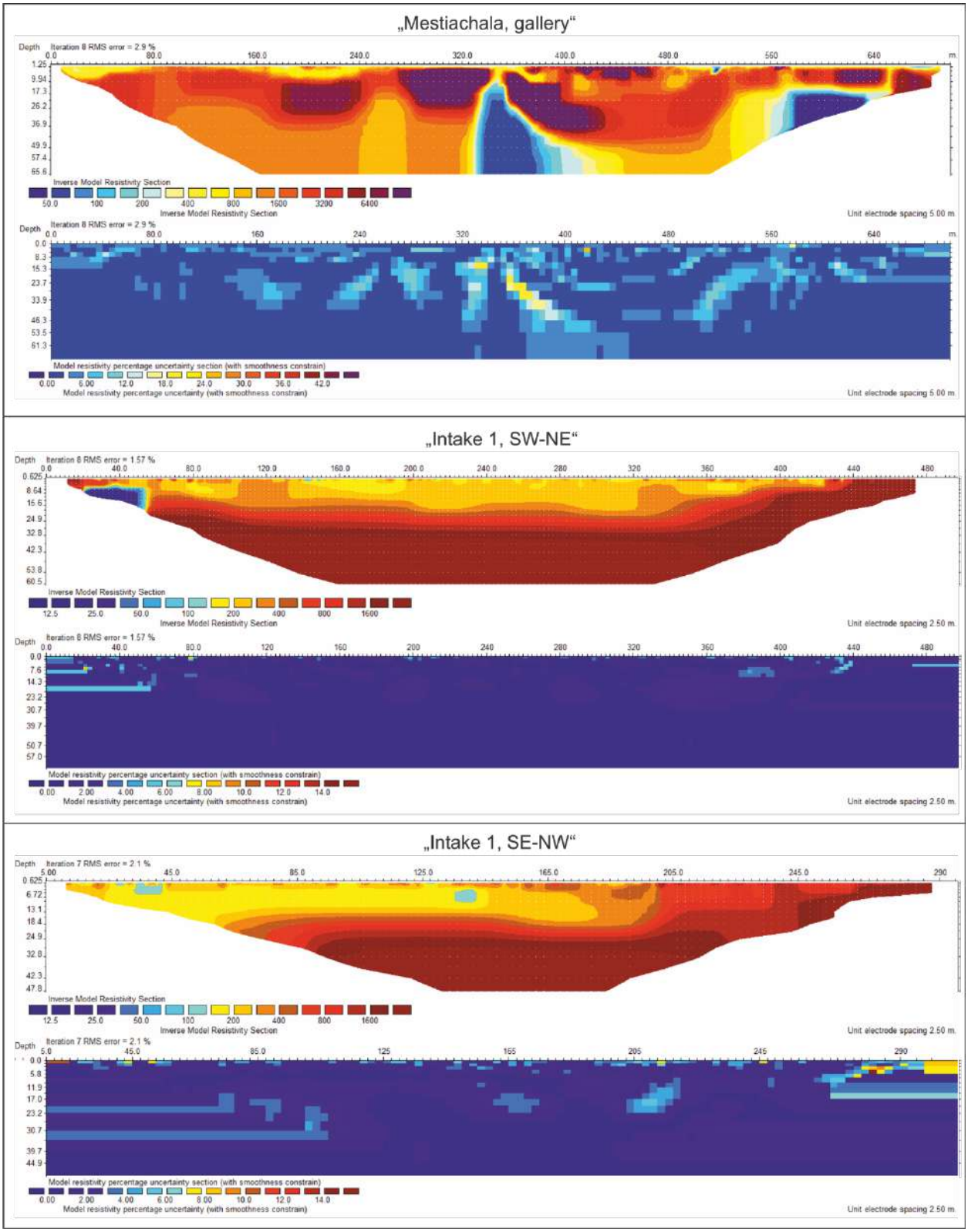

Fig. 6-4: Display of the geoelectrical transects “Mestiachala, gallery”, “Intake 1, SE-NW” and “Intake 1, SW-NE” after robust inversions: “Inverse model resistivity section” plot without topography on top and “model resistivity percentage uncertainty section” plot on the bottom.

After eight iterations (transects „Mestiachala, gallery" and "Intake1, SW-NE) and seven iterations (transect "Intake 1, SE-NW"), respectively, an average RMS error of 1.6 % to 2.9 % was achieved. In Fig. 6-4 the three transects are displayed in form of an "inverse model resistivity section" and a "model resistivity percentage uncertainty section". The upper section of each transect shows the inversion results and the lower the corresponding distribution of the block uncertainties. For a better comparison, the topography is excluded.

By contrast to Fig. 6-4, the following Fig. 6-5 and Fig. 6-6 show the resistivity models including the topographical data.

The transect "Mestiachala, gallery" runs on the orographic right side of the Mestiachala river and basically follows the construction road. After about 560 m length the transect reaches the gallery and passes at river level.

The resistivity values of the model (Fig. 6-5) vary between 19 Ωm and 140,000 Ωm. Based on the resistivity distribution different areas can be distinguished along the profile. Zones with low resistivities between 20 Ωm and about 300 Ωm are represented in bluish colours. Two areas are located in the deeper part of the profile as well in the middle section between 320 m and 410 m as in the north-eastern part between 560 m and 650 m. Medium resistivities between 300 Ωm and about 1600 Ωm are defined by yellow to orange colours and can also be found in the deeper part of the profile between the low resistivity areas. These deeper parts are differentiated from the upper layers by a clear border. The shallow part of the profile between the surface and a depth of about 10 m to 50 m is characterized by very inhomogeneous resistivities between 50 Ωm and 140,000 Ωm (blue to magenta).

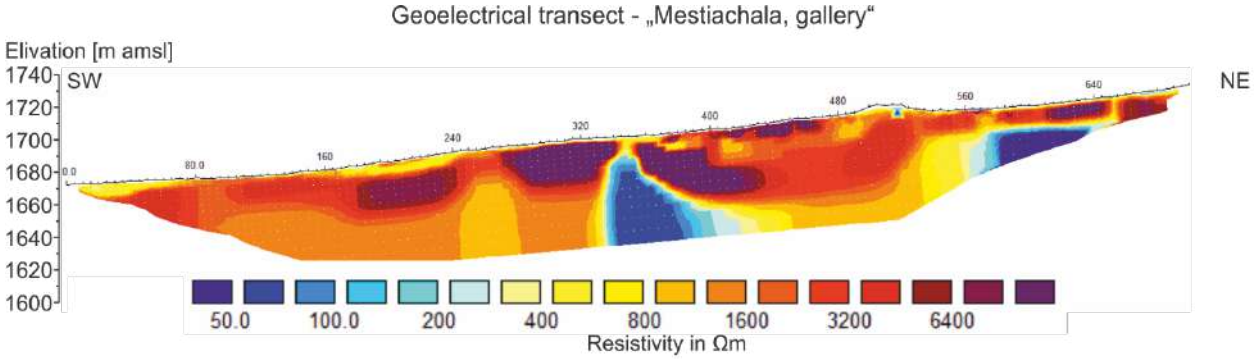

Fig. 6-5: Resistivity model of the geoelectrical transect „Mestiachala, gallery". Resistivity contour values are defined in logarithmic intervals.

The transect "Intake 1, SW-NE" starts next to the desander. It reaches the event deposits at about 30 m. The northern border of the deposits is at about 440 m. The transect "Intake 1, SE-NW" begins close to the riverbed and near the approximate position of the intake 1. The transect runs up the event deposits and reaches the original slope deposits at about 240 m length along the

transect. Both transects intersect mutually more or less orthogonally. The positions are shown in Fig. 6-6 and in the maps in Attachment 9.

Both models show resistivity distributions that are characterized by a higher lateral homogeneity compared to the transect “Mestiachala, gallery”. The total resistivity values are in the range between 12 Ωm and 320,000 Ωm. Low resistivities are also represented in bluish colours but vary in this case between 12 Ωm and about 150 Ωm. There is only one zone to be found that is characterized by these properties. It is located between the positions 20 m and 55 m along the transect “Intake 1, SW-NE”. High resistivities are defined by more than 1,600 Ωm (dark red) and are detected in the deeper parts of both profiles. The zones with low and high resistivity values are capped by layers with medium resistivity values between 150 Ωm and 1,600 Ωm (yellow to red colours).

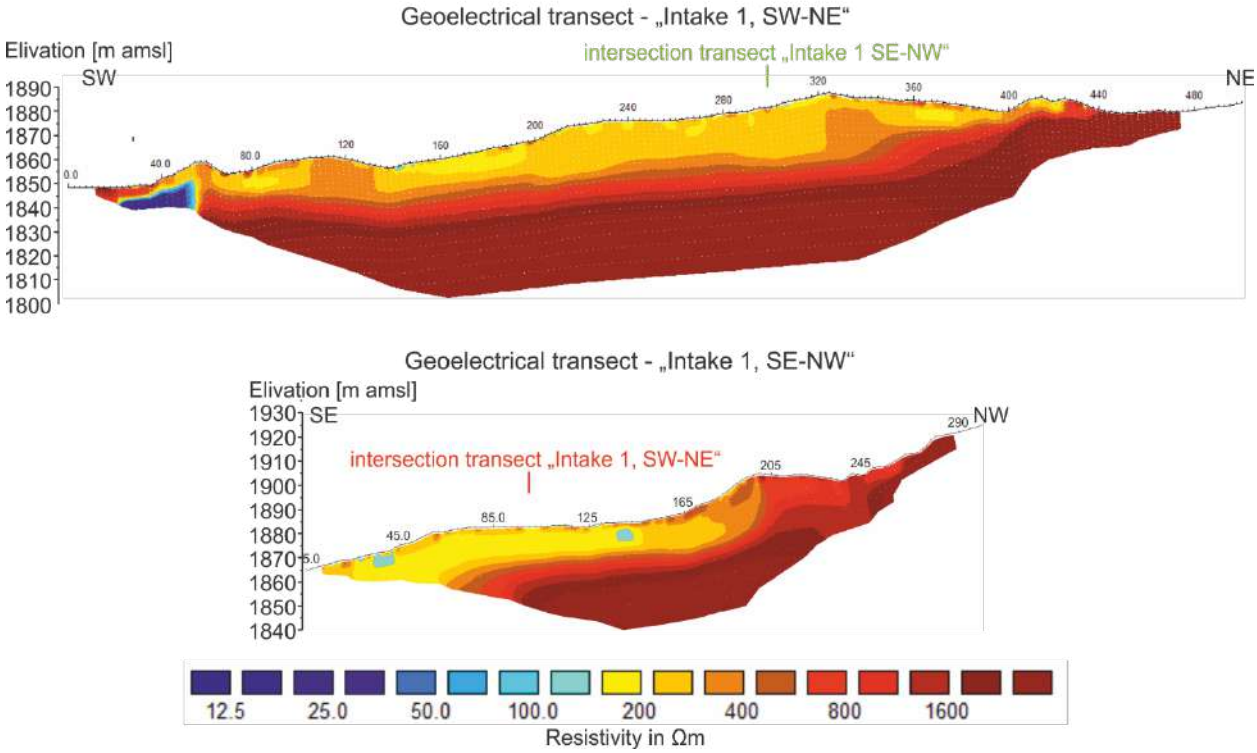

Fig. 6-6: Resistivity model of the geoelectrical transects „Intake 1, SW-NE” and “Intake 1, SE-NW”. Resistivity contour values are defined in logarithmic intervals. The transects intersect orthogonally at the marked locations.

6.4 Evaluation and geological interpretation of the ERT results

The interpretation of geoelectrical measurements generally starts with the calibration process. In the absence of additional information from soil investigation drilling in the Mestiachala valley or calibration measurements on rock samples, a detailed geological mapping along the transects was carried out. Geoelectrically measured resistivities of surface material was compared to findings in the geological mapping process. This dimension could then be transferred to

subsurface ERT results. These results and the geological interpretation along the transects are described in the following chapters and are displayed in Attachment 9.

6.4.1 Longitudinal valley transect "Mestiachala, gallery"

The Mestiachala valley is filled with colluvial and alluvial sediments which are a weathering product of surrounding Jurassic and Palaeozoic rock formations. Depending on the origin and the transportation process the petrographic composition and the grain size distribution of multiple layers are significantly different. This diversity is represented in a very heterogeneous resistivity distribution in the shallow part of the profile. The border of the sediments to the solid rock is located in a depth between 10 m to 50 m (estimated lower border marked with white broken line).
Scattered low resistivities up to 800 Ωm very likely represent either fluvial deposits with smaller grain sizes (gravel) or slope debris of high fragmented clay slates. Areas with resistivities between about 600 Ωm and 3,000 Ωm can be interpreted as poorly sorted fluvial sediments or slope debris with a mixture of clay slates and Granite components. Higher resistivities possibly stand for very blocky material and/or mostly granitic components. Partly, the pore water content might also be low (e. g. location above river level).

In this part of the Mestiachala valley, clay slates and quartzite in alternating sequences outcrop at the surrounding rockfaces. Therefore, these formations are also expected to underlay the valley sediments. Resistivities between about 50 Ωm to 300 Ωm are representative of the Mestiachala clay slates, values between 800 Ωm und 1,600 Ωm for the quartzite. Areas with resistivities between 300 Ωm and 800 Ωm are interpreted as a tighter alternating sequence of clay slates and quartzite.

6.4.2 Transects at the impact area at intake 1

At the impact area two mutually orthogonally crossing ERT transects were carried out. Along these transects a more or less homogenous top layer with resistivities between 100 Ωm and 300 Ωm was detected and interpreted as the deposits of the 2019 event. The deposits mainly consist of clay slates with a high portion of pyrite. Granite components are rare within the main body of these deposits. At the lateral borders of the deposits the resistivities rise to about 1,200 Ωm. These parts (transect "Intake 1, SE-NW" in section between around 200 m and 265 m and transect "Intake 1, SW-NE" in section between 425 m and 440 m) are interpreted as remobilized talus and fluvial deposits (mainly granites and gneisses) during the impact. The event deposits reach a thickness between about 5 m and 25 m. Both transects show syncline structures at the lateral borders between the main deposits and the remobilized sediments which were formed during the impact: when the falling and flowing mass hit the valley ground it pushed the existent valley deposits aside.

The main part of the bedrock along both transects shows resistivities between 300 Ωm and over 100,000 Ωm. These parts are interpreted as Palaeozoic gneisses corresponding to the surrounding geological formations. The linear increase of the resistivity in the first 10 m to 20 m of the gneisses can be explained by a weathered top layer.

In the very southwest of the transect “Intake 1, SW-NE” bedrock with a very low resistivity (10 Ωm to 100 Ωm) is detected underlying the valley sediments. Similar to the transect “Mestiachala, gallery” this part is interpreted as Jurassic clay slates, since outcrops can be found in the vicinity of the riverbed. Since the Main Caucasus Thrust (MCT) represents the border between the Jurassic and the Palaeozoic rock formations, the MCT can be located more or less vertically after about 55 m of the mentioned transect.

7 Modelling of high-magnitude debris flows

7.1 Overview of the performed simulations

Within the simulation study two different simulations were performed:

The first simulation aimed to back-calculate the 2019 compound rock-ice avalanche and subsequent debris flow event in the Murkvami tributary and thus to support the in-situ estimation of volumes released as a rock avalanche, of material deposited along the track as well as at the mouth of Mestiachala valley.

The second simulation aimed at unveiling volumes, pressures and flow velocities of a hypothetical debris flow in the Mestiachala valley based on a 1-in-30-year (1-in-100-year) design discharge. The modelling results indicate possible impacts on the infrastructures of HPP 1.

7.2 Introduction to Simulation tool r.avaflow

The software r.avaflow is a flexible and multi-functional, GIS-based open source computational framework for the simulation of geomorphic mass flows. The developers of r.avaflow have focused on the development of a novel simulation tool for the motion of debris flows, snow avalanches, rock avalanches, and process chains consisting of more than one component (compound events). In contrast to most other software packages available this tool offers a two- and three-phase flow model and considers entrainment and deposition of material along the path (MERGILI 2014-2020). Nonetheless, it has to be mentioned that even the best models only produce an approximated and generalized view of reality (MERGILI and PUDASAINI 2014-2020), which in turn means that modeling results have to be carefully interpreted and supplemented by in-situ field studies and remotely-sensed data so that overall findings are reliable and represent reality the best possible way.

7.3 Back-calculation of the 2019 event

7.3.1 Event description

On 25 July 2019 a rock-ice avalanche was released in the Murkvami tributary of the Mestiachala valley (see Section 3.3 of the October 2020 Interim Report). Satellite images and on-site inspections showed that within a short period of time two solid masses were released in the Murkvami tributary. This is proven due to the clearly visible superposition of two layers at the confluence of the tributary and the Mestiachala valley and by drone imagery conducted during the August 2020 field campaign. The released masses hit the glacier tongue of Murkvami glacier, entrained a considerable amount of ice moved down the tributary in terms of a debris flow. Some of the material was deposited along the track when flowing downwards, and the majority of the flowing mass was deposited at the confluence of the tributary and the main valley, destroying the intake infrastructure of HPP 1 situated in the area around the confluence.

7.3.2 Generating data for simulation

The standard process for determining the precise location of the release areas and their volumes is to subtract a current digital elevation model (DEM) from a DEM before the event. Because a current DEM was not available and the existing DEM from the year 2007 has a spatial resolution of 12.5 meters, the overall accuracy of the simulation results has to be carefully interpreted and mirrored against the results of the field survey. As there is no recent and high-resolution DEM available covering the Murkvami valley, the release areas and their volumes had to be estimated based on the analysis of drone and satellite imagery and from additional information obtained during the field campaign. For the release areas, a total volume of around 1.6 million m³ was assumed. This volume was divided into 1.3 million m³ for the main release area (T-R1 in Fig. 3-5) and the remaining for the second release area (T-R2 in Fig. 3-5). As terrain analysis resulted in the assumption that the smaller area was released with a certain time lag after the triggering first release, a time lapse of 120 seconds was implemented in the model. The release areas were assessed and defined using the geoinformation software ArcGIS and were then implemented in the simulation tool.

7.3.3 Simulation input

The simulations with r.avaflow build on the topography, represented by a DEM, and on particular sets of initial conditions and model parameters (MERGILI et al. 2020: 99). For the DEM, a 12.5 m resolution digital elevation model (DEM) provided by an earth observation satellite, the Advanced Land Observing Satellite (ALOS) from the Japan Aerospace Exploration Agency, was used. The aim of this satellite program is to generate and contribute, amongst other things, to disaster monitoring. The satellite is equipped with three remote-sensing instruments. The PALSAR (Phased Array type L-band Synthetic Aperture Radar) instrument is suitable for day and night land observations, regardless of the weather (Japan Aerospace Exploration Agency 2008). The DEM was generated using Interferometric synthetic aperture radar (InSAR) (ARAMBERI et al. 2020: 1). The DEM covers the entire area of interest. A higher resolution of the DEM would have been advantageous to simulate the mass movement, but no other data was available at the time of processing.

The values of the model parameters were selected from existing literature according to the experiences from previous simulations with r.avaflow for other study areas, and were adapted to the conditions in the Mestiachala area. The selected parameter values are summarized in Tab. 7-1.

The flow friction of the rock-ice avalanche is mainly characterized by the basal friction of the solid material and by the ambient drag coefficient. By the ambient drag coefficient, the air resistance is considered.

The basal friction angle is a decisive parameter for the simulation. Due to the local conditions in the tributary, two different values for the basal friction angle were assumed along the transit area of the landslide. By dividing the transit area using two different values, optimal simulation results were generated.

The entrainment of ice is determined using the entrainment coefficient. This coefficient is used to derive the entrainment rate of basal material.

Tab. 7-1: Model paramters; Tributary

Parameter	Unit	Value
Solid material density (grain density)	kg/m³	2,700
Ice material density	kg/m³	1,000
Internal friction angle	Degree	35
Basal friction angle	Degree	14; 12
Ambient drag coefficient	-	0.02
Entrainment coefficient	-	10^{-7}

7.3.4 Results of the simulation

The back-calculation of the mass movement aimed to simulate the observed conditions on site (by evaluation of satellite imagery/mapping on site) as accurately as possible. A parameter optimization was performed to achieve a high agreement between the most important observed output parameters impact area and deposited volumes. Since there are no eyewitness reports and no monitoring stations, the simulation can provide the only information about assumed (frontal) velocities and travel times of the mass movement.

7.3.4.1 Deposition

In Fig. 7-1 the deposition heights of the mass movement are given along the entire track. Below the middle moraine (dividing Murkvami and Banguriani valleys) larger deposition areas are located, which is partly due to the lower inclination in this area. Similar deposition areas were also mapped along the transit route of the rock-ice avalanche in the Murkvami tributary during the field survey on 16 August 2020. Please note that the spatial coverage of the model does not exactly match the inspected coverage in the landscape, which is an artifact of the discussed coarse resolution of the underlying DEM. Thus, the results of the simulation reflect the observed deposition areas quite correctly. Modelled deposit heights of up to 10 meters are consistent with field measurements during the survey. Depositions south-west of the middle moraine are shown and correspond to the observed overtopping of the medial moraine during the event, these depositions have a maximum height of 2.2 meters.

The maximum deposition heights were obtained at the confluence to the Mestiachala valley, where the main part of the 2019 event was deposited. Deposition heights reached values of up

to 18-20 meters (including pore space), which is in line with the results from the geoelectric survey as well as the in-situ measurements performed during the field survey.

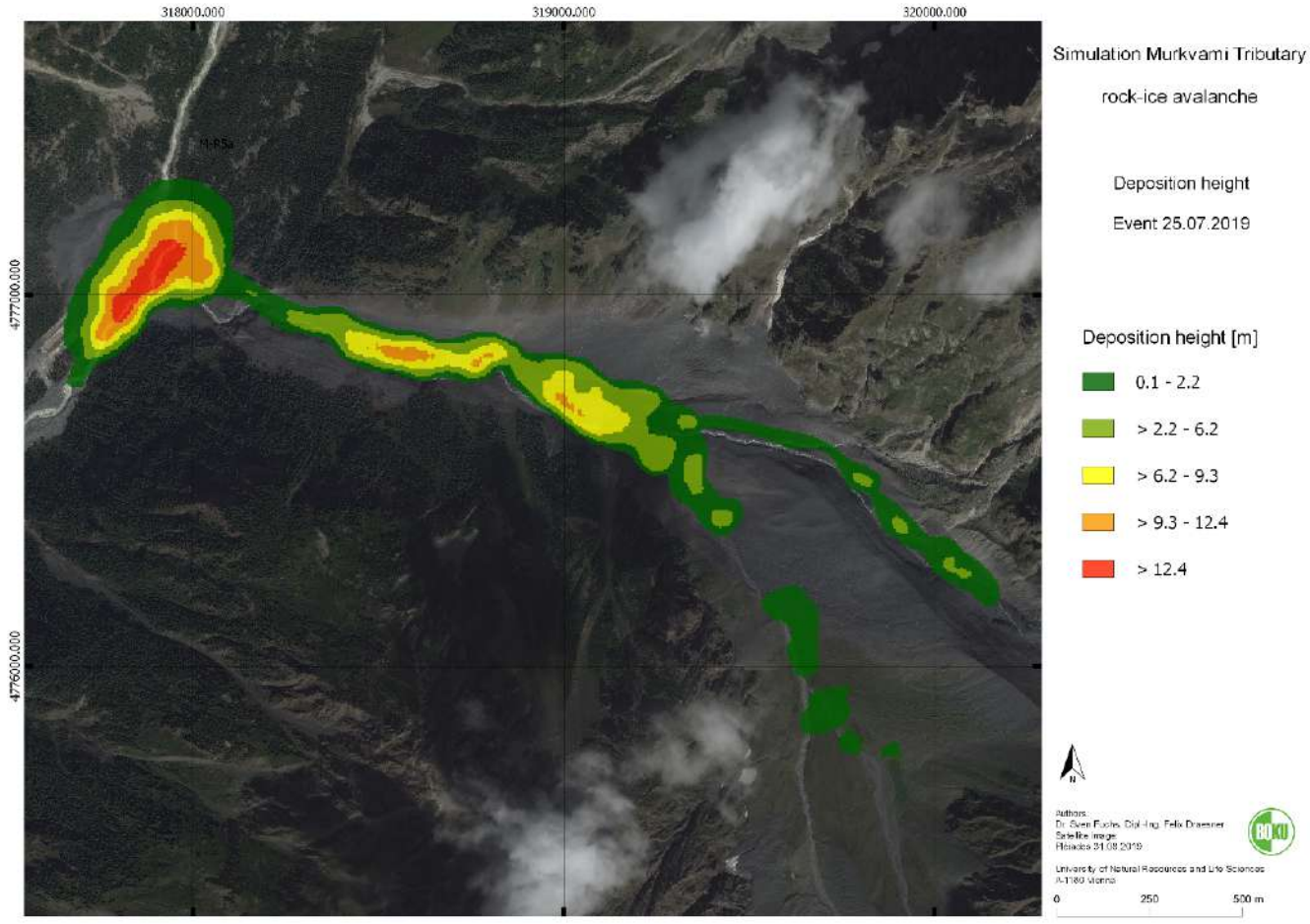

Fig. 7-1: Simulation Murkvami Tributary; Deposition height

7.3.4.2 Velocity

In Fig. 7-2 the maximum flow velocity over the entire time interval of the mass movement is shown. The initial rock-avalanche rapidly increased in speed after their release and moved downslope with frontal velocities exceeding 27.5 m/s. When reaching the glacier tongue velocities between 20.7 and 27.5 m/s were observed, as well as an entrainment of ice in the flow.

With increasing distance from the release areas, the mass movement decreases in speed due to the lower inclination. Just before the tributary hits the main valley, the slope gradient increases again significantly and consequently, a renewed increase in speed was observed.

The mass movement reached an average velocity of 15 m/s (54 km/h), therefore, once released, it takes around 240 seconds (4 minutes) for the material to reach the final deposition area at the mouth of the Tributary.

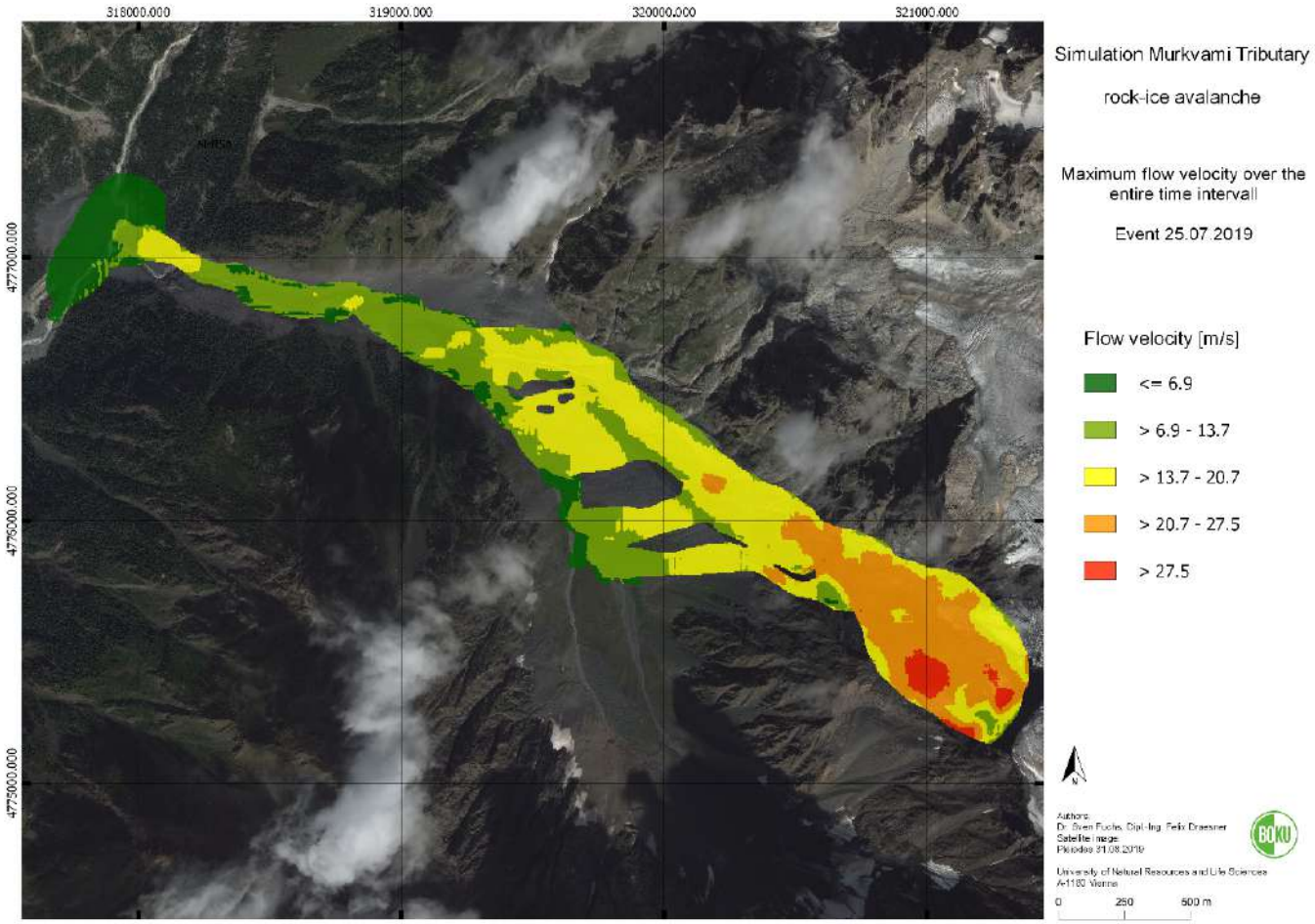

Fig. 7-2: Simulation Murkvami Tributary; Flow velocity

7.3.4.3 Pressure

Fig. 7-3 shows the maximum flow pressures over the entire time interval of the mass movement. Maximum flow pressures of up to 1,000 kN/m² were reached in the steep section just before the deposits located in the Mestiachala valley (E318,137/N4,777,017). The location of the former intake (E317,873/N4,777,062) also shows very high flow pressures of up to 500 kN/m². The flow pressure decreases successively in north-west direction with increasing distance towards the present channel.

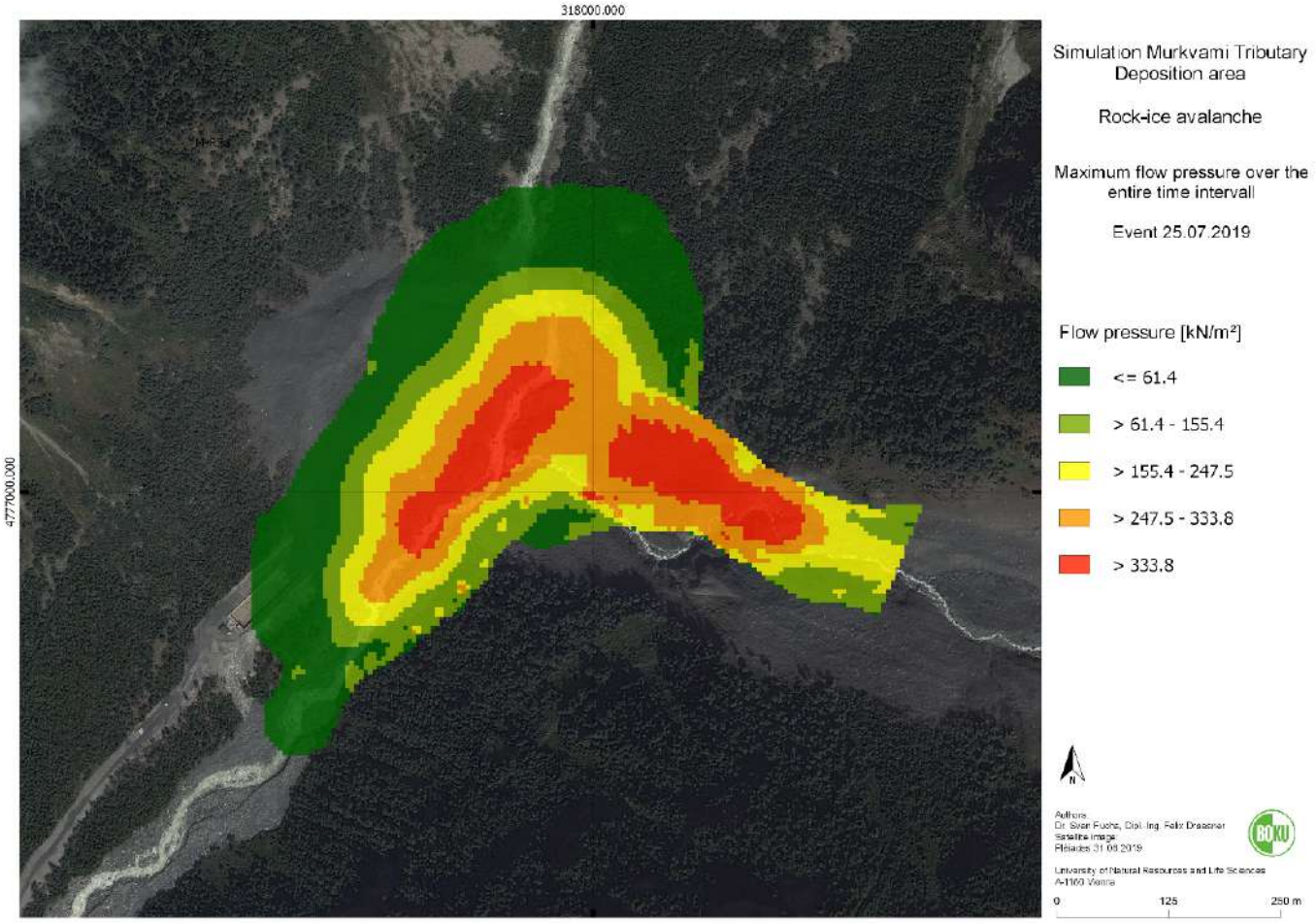

Fig. 7-3: Simulation Tributary; Flow pressure

7.4 Simulation of a hypothetical debris flow in the Mestiachala valley

7.4.1 Event description

The depositions of the 2019 mass movement from the Tributary only briefly dammed the main channel originating from Lekhziri. Because there was only evidence for little ponding observed during the field survey, it is assumed that the river flow though the deposited material immediately after the blocking. Consequently, only a small part of the deposition was eroded along the former flow path whereas most of the deposited material was not mobilized. This was also evident during the field survey and when assessing the available satellite imagery. The material deposited along the track between the former intake 1 and HPP 1 provided evidence that the rock content of the following debris flow mainly originates from depth erosion and lateral erosion of the river course. Lateral erosion was observed especially on the orographic right side of the channel. The avalanche gallery was scoured due to a missing foundation. North of the gallery, slope erosion occurred and has exposed the penstock of the HPP (Fig. 7-4). The following simulation aims to represent a 1-in-30 (1-in-100)-year design discharge according to the

HYDROCONSULT report (2015), leading to a debris flow so that volumes, velocities and pressures can be assessed for the HPP infrastructure. Acknowledging the fact that in the Hydroconsult report extreme values are missing, the 1-in-30-year discharge might be underestimating in-situ situations. To take this into account, the 1-in-100-year design discharge is therefore used for comparison, which are given in brackets in the following sections. The current topography of the Mestiachala valley was used as the basis for the simulation.

Fig. 7-4: The exposed penstock is located directly at a bend in the channel (317048/4776420). Due to the discharge in the riverbed, this location is particularly susceptible to possible erosion (Photo by Resinger 2020).

7.4.2 Simulation input

For the DEM, a 1.0 m resolution digital elevation model (DEM) provided by the client was used. This high-resolution DEM was created by a drone flight in the summer 2020. The DEM covers the area from the former intake 1 to the powerhouse of HPP 1. The area south of HPP 1 as well as the areas of Chalaati valley and Murkvami valley are not covered by the DEM.

The values of the model parameters were selected from existing literature according to the experiences from previous simulations with r.avaflow for other study areas and were adapted to the conditions in the Mestiachala area. The selected parameter values are summarized inTab. 7-2.

The basal friction angle is a decisive parameter for the simulation and is selected due to the local conditions in the Mestiachala valley.

The 1-in-30 (1-in-100)-year design discharge is assumed with 104.9 m³/s (143.1 m³/s) based on existing data provided in studies performed earlier during the construction of the hydropower plant (HYDROCONSULT 2015: 4). The discharge was divided in 2/3 and 1/3 in order to account for the different water volumes available from Lekhziri catchment and from the Tributary. The higher discharge [2/3 => 69.93 m³/s (95.4 m³/s)] originates north of the former intake 1 from the Lekhziri catchment and the lower discharge [1/3 => 34.97 m³/s (47.7 m³/s)] originates from the Murkvami tributary. These two discharges confluence at E317,896/N4,777,026 and result in the 1-in-30 (1-in-100)-year design discharge according to HYDROCONSULT (2015). The loose material in the channel is available as entrainment. As the simulation was aimed to unveil flow conditions at critical HPP constructions, particular attention was given to the area along the current avalanche gallery, the area of the exposed penstock and to the area surrounding the powerhouse of HPP 1. The simulation runs until the loose material for the entrainment has been completely eroded.

Tab. 7-2: Model parameters; Mestiachala

Parameter	Unit	Value
Solid material density (grain density)	kg/m³	2,700
Internal friction angle	Degree	35
Basal friction angle	Degree	9
Ambient drag coefficient	-	0.02
Entrainment coefficient	-	10^{-7}

7.4.3 Results of the simulation

7.4.3.1 Pressure

In Fig. 7-5 the maximum flow pressure distribution is shown over the entire time interval of the debris flow simulation. It can be clearly seen that especially the constrictions along the flow path as well as the sudden changes of direction are under greater pressure, reaching values of up to 350 kN/m². The areas of the exposed penstock, next to the avalanche gallery as well as around the powerhouse of HPP 1 are analysed in detail.

Due to the recorded damages of the gallery by the 2019 event there was evidence for significantly high flow pressures these sections are exposed to. The simulation results confirm these assumptions that especially in these sections high pressures of up to 170 kN/m² (180 kN/m²) act on the channel bottom and the slope next to the gallery. Furthermore, the embankment at the exposed penstock is exposed to particularly high pressures.

The simulation shows that the channel bottom south of the gallery (E316,925, N4,776,230 – E316,825, N4,776,010) is particularly exposed to strong pressures for around 250 meters in length. The pressure decreases south-west of the highly pressured channel bottom.

A further significant increase is observed next to the constriction (suspension bridge) right before the power house, especially on the orographic right side. High pressures exceeding 300 kN/m² (400 kN/m³) might occur. These high pressures are to be expected due to the topography (slight left turn of the channel bed) and were therefore confirmed by the simulation. At the overflow of the weir, a short decrease of pressure is detectable. This pressure decrease is mainly due to the overflow, which is also confirmed by the immediate increase downwards the weir. The topography around the power plant is more flat, which leads to spreading of the flow into a wider area with a corresponding decrease in flow pressure.

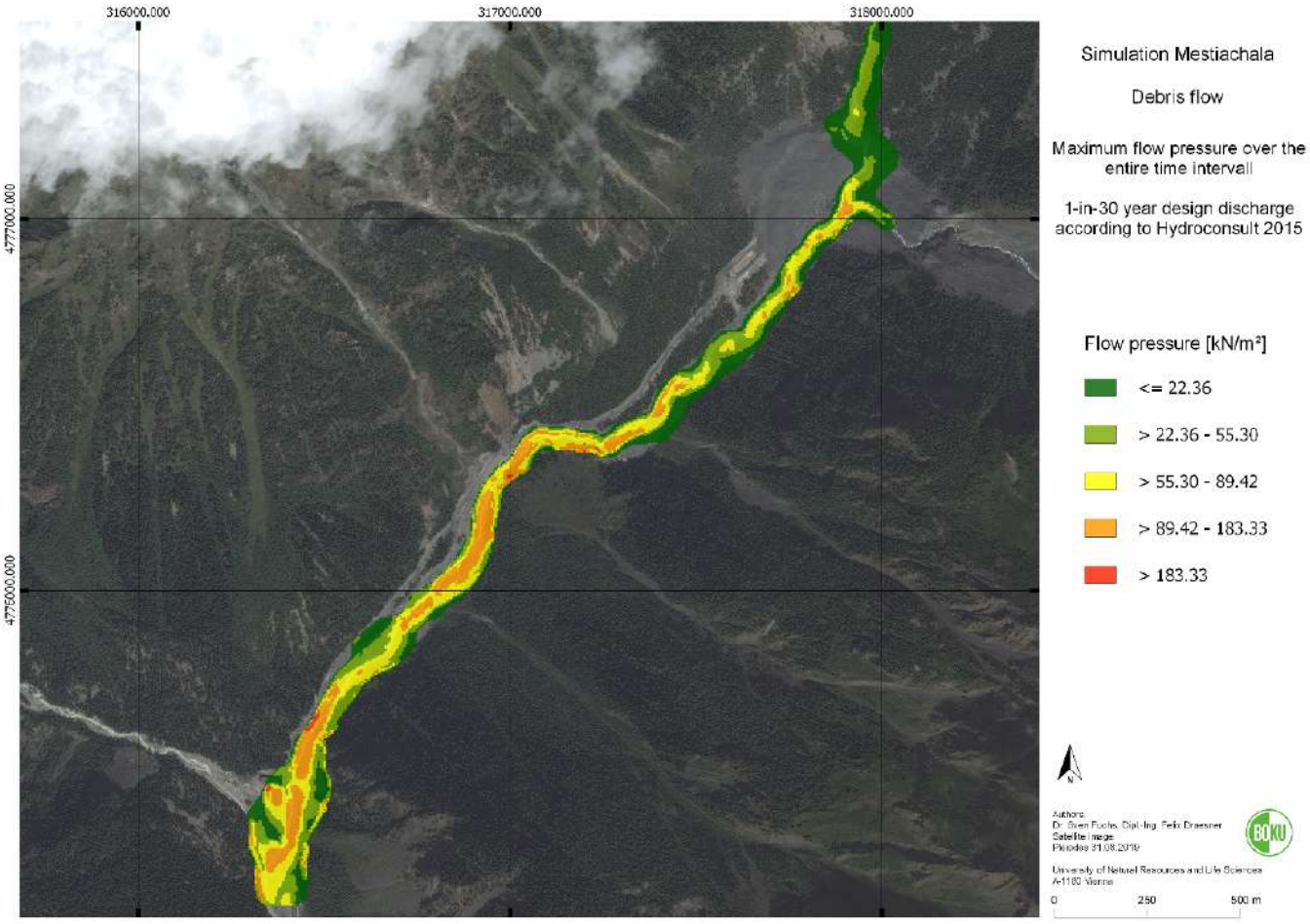

Fig. 7-5: Simulation Mestiachala valley; Flow pressure

7.4.3.2 Flow heights

In Fig. 7-6 the maximum flow heights are illustrated over the entire time intervall of the debris flow simulation. North of the deposition area a small ponding was observed during the field survey, which has also been obtained by the simulation results. The 1-in-30-year design discharge is expected to mobilize only few material of the deposition area. As already observed in the field, most of the material mobilized by the debris flow has its origin between the former intake 1 and

the powerhouse of HPP 1. The flow successively erodes material and thus develops into a debris flow. Between the deposition area and the sharp left turn towards the avalanche gallery, the flow heights vary between 0.1 meters and 2.0 meters (2.5 meters) (maximum). Next to the exposed penstock, the flow height is up to 3.2 meters (3.8 meters) due to the constriction of the channel. On the orographic right side next to the gallery, maximum flow heights of 2.3 meters (2.9 meters) are simulated. The flow heights increase significantly before the constriction at the suspension bridge, partly due to the increasing amount of solid material in the flow. After the weir, the lateral expansion of the flow increases to east and west, filling the desander and the parking area. Flow heights exceeding 5.5 meters (6.5 meters) are measured during the simulation. It has to be mentioned that depth erosion of up to 2 meters has been modelled just after the weir. Directly around the weir lower flow heights were calculated because depth erosion is not possible at this point. After the weir, the flow cross section spreads due to the flat topography and results in lower flow velocities and therefore to increasing flow heights in time. The increase in flow heights is also due to the increased content of solids, which has gradually increased up to this point. The desander at E316,361, N4,775,427 is filled by the flow after the flow height exceeds the surrounding wall (see also Fig. 7-6).

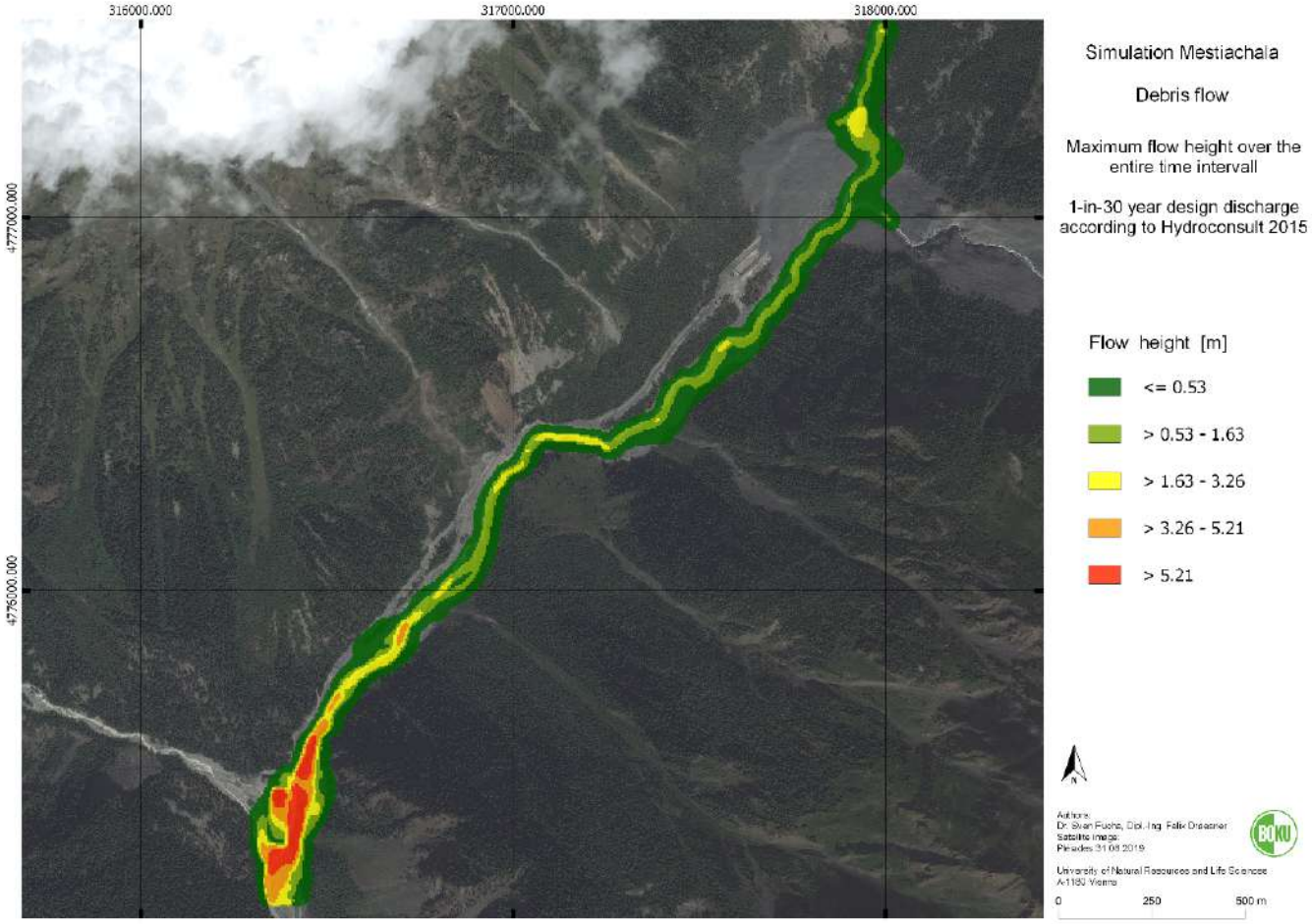

Fig. 7-6: Simulation Mestiachala valley, Flow height

7.4.3.3 Flow velocity

Fig. 7-7 illustrates the maximum flow velocity over the entire time interval of the debris flow simulation. Values of up to 15 m/s (16 m/s) are reached with high flow rates downwards the inflow from Murkvami valley. These high flow velocities lead to increased sediment entrainment between the inflow of the Murkvami valley discharge (E317,896, N4,777,026) and the orographic right turn at E317,249, N4,776,370. Between this position and the exposed penstock (E317,048, N4,776,420) the flow velocities vary between 8.4 and 11.0 m/s (same values as the 1-in-100-year design discharge), increasing again after this location. It is noticeable that the flow velocity decreases after the weir because of the lateral spreading of the cross section due to the flat and wide topography.

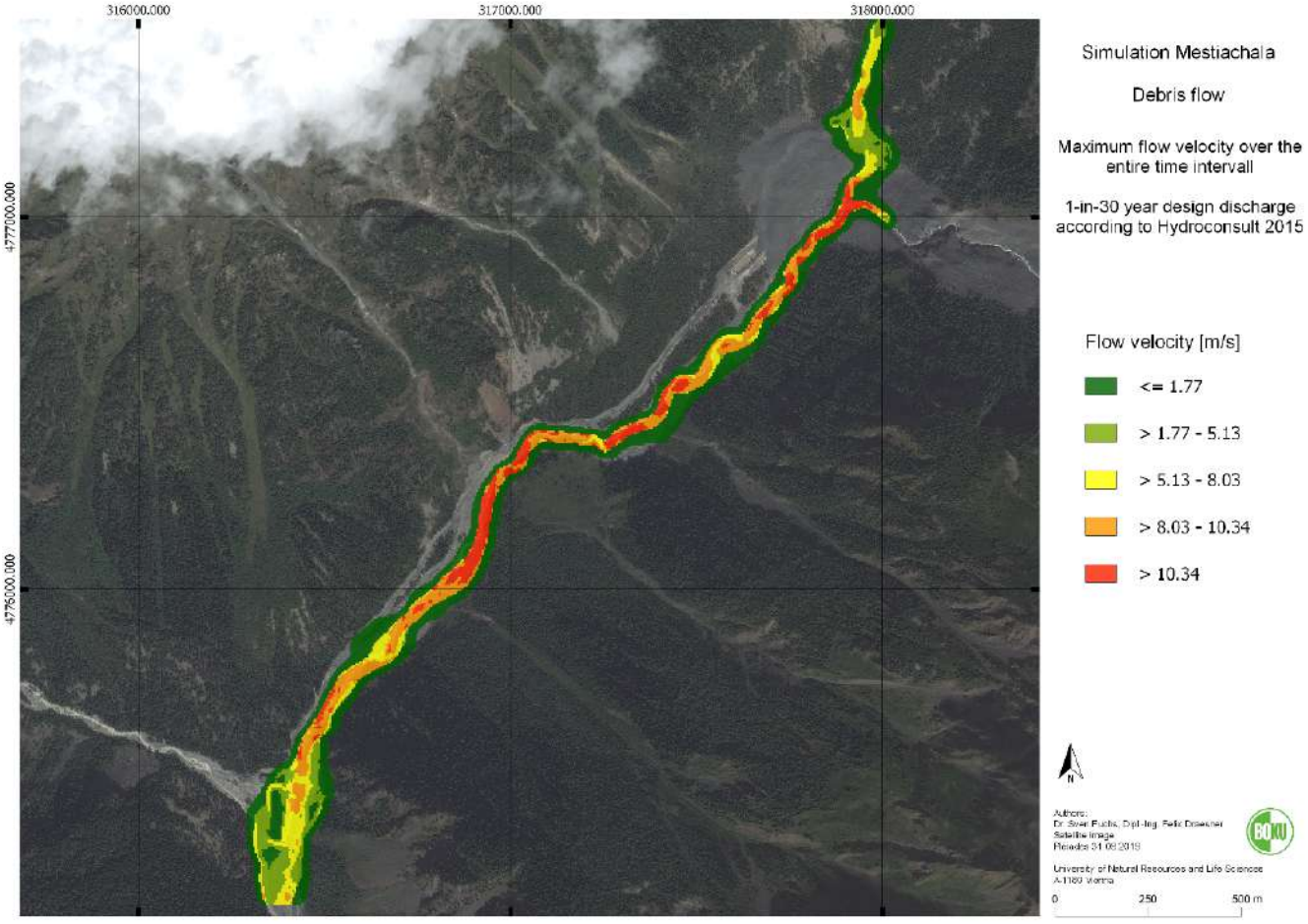

Fig. 7-7: Mestiachala valley; Flow velocity

7.4.3.4 Time span

Fig. 7-8 shows the development of the debris flow over time. Each sequence illustrates the successive situation in successive time intervals of 100 seconds. From the different sequences it can be seen that the flow is very fast at the beginning and gradually loses speed. The debris flow reaches the powerhouse after 380 seconds (6 minutes and 20 seconds). The overflow into the desander is predicted after 480 seconds.

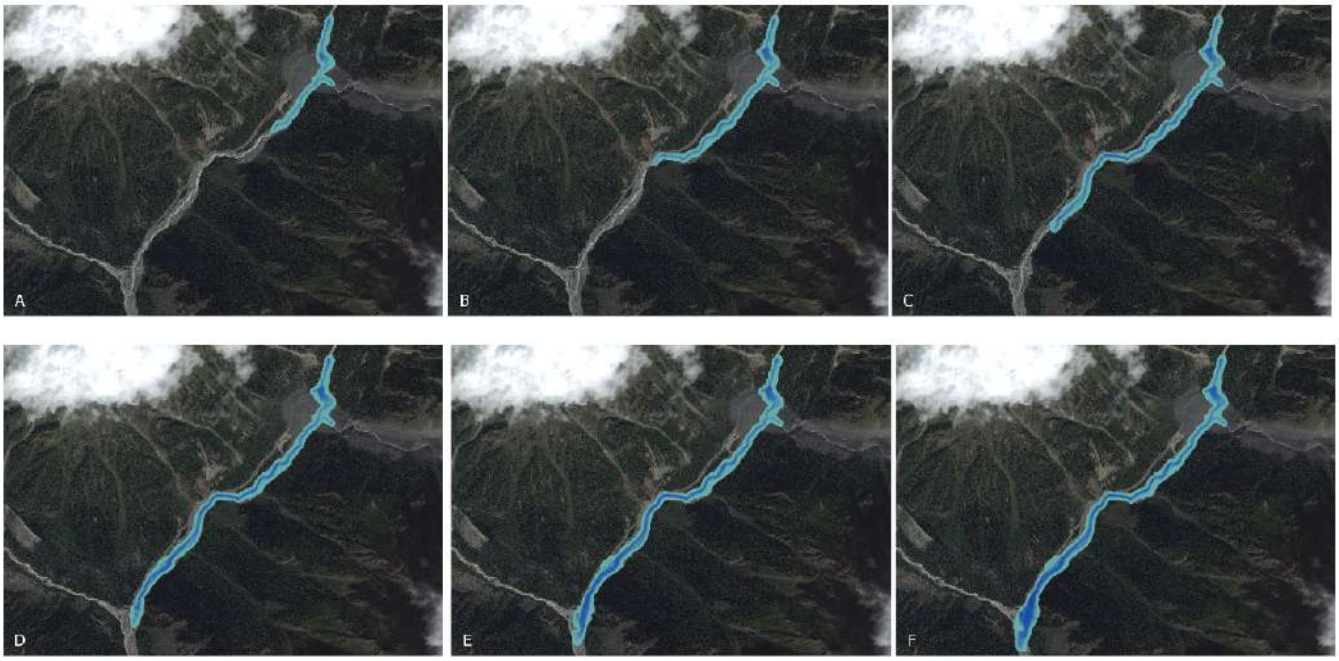

Fig. 7-8: Mestiachala valley; Developement of the debris flow in time; A=Situation after 100 seconds; B=Situation after 200 seconds; C=Situation after 300 seconds; D=Situation after 400 seconds; E=Situation after 500 seconds; F=Situation after 600 seconds

7.5 Conclusions

In Tab. 7-3 and Tab. 7-4 the simulated values at specific locations are summarised. These values give an indication of possible impacts occurring during simulated events. For the possible new location for intake1, impacts from both simulations are provided below.

Tab. 7-3: Maximum simulated values; Murkvami tributary simulation.

	Deposition height	Flow pressure	Flow velocity
Former intake1	Up to 18.0-20.0 m	Exceeding 700 kN/m²	Exceeding 13 m/s
New intake1	Up to 4.0 m	Up to 60 kN/m²	Up to 6 m/s

Tab. 7-4: Maximum simulated values; Mestiachala valley simulation.

	Flow height	Flow pressure	Flow velocity
New intake1	In a range of 3.0 – 3.5 m	In a range of 60 – 70 kN/m²	In a range of 8 – 10 m/s
Exposed penstock	In a range of 2.0 – 3.5 m	In a range of 110 – 125 kN/m²	In a range of 11 – 13 m/s
Gallery	In a range of 2.2 – 3.1 m	In a range of 110 – 135 kN/m²	In a range of 11 – 13 m/s
Suspension bridge	In a range of 5.2 – 6.6 m	In a range of 120 – 250 kN/m²	In a range of 9 – 11 m/s
HPP	In a range of 4.0 – 7.0 m	In a range of 100 – 140 kN/m²	In a range of 8 – 10 m/s

It has been proven that the software r.avaflow is capable for showing the behavior of compound mass movement processes in the study area, and results are in line with other technical methods (e.g., geoelectrics) and interpretation of satellite imagery as well as results of ground-based field surveys. Based on the simulation results it can be estimated how a debris flow can develop and which flow heights, flow velocities and flow pressures may be expected. The modelled results provide reference values for a possible comparable event. However, as these results are modelling results they only reflect reality to a certain point, which means that for planning and implementation of any kind of mitigation, additional in-depth studies are required. Generally, using any kind of model for prediction of any kind of hazard is subject to many simplifications and as such, only rough estimations can be given which may be subject to uncertainties with respect to precision and accuracy.

8 Rockfall simulation and rock slope stability estimation

In this chapter, active rockfall areas are described which have a direct impact on the HHP 1 structures. These “Group-1-events” (minor rockfalls or lowermost range of medium size rockfalls) occur quite frequently and have to be mitigated in one or the other way (see Chapter 4.3 and 12.1.1). In addition, we will have a closer look on larger slope instabilities, which can lead to medium or large rockfall or even have impact as “Group-2-events”, i.e. a very large rockfall, as singular event or as part of a cascading event.

8.1 Rockfall simulation

In general, large parts of the rock outcrops in the catchment are prone to release of rocks and boulders. Alost the entire slopes are potential release areas. The occurrence probability and magnitudes, however, differ. Two highly-active run-out zones were determined at M-D4 and M-D6, which spatially overlap with the HPP structures (Chapter 4.3). Additionally to the field survey, these were investigated with software simulations in order to verify potential process intensities and run-out areas as well as to assess possible mitigation alternatives that are economically feasible. Despite, also other release and deposition areas may pose a threat to HPP facilities such as M-D8, however, these were not modelled as they were evaluated being less active, partly because of a more effective forest protection (see Chapter 4.3.1). In any case our results cannot replace a final design for protection measures at the present state.

8.1.1 Method of rockfall simulation - GeoRock 2D

8.1.1.1 General information

The falling motion of a boulder along a rocky slope depends on many factors which are challenging to be numerically expressed in a model. The trajectories of boulders depend on the geometry of a slope, on the shape of the boulder and on its initial velocity when detached from the slope, and also on the energy dissipation during impacts on the slope due to a parabolic trajectory of particles in motion. The moving boulders can slide, roll or bounce downstream depending on their shape (flattened or rounded) and on the gradient of the slope.

The energy dissipated due to impacts is generally different, varies with the characteristics of motion and depends on the mechanical characteristics of the boulder and on the materials present along the trajectory (rock, soil, vegetation) and influencing the motion of the boulders. The geometry of the slope, moreover, and therefore the nature of the outcropping materials are temporally variable. This leads to variations of the vertical and horizontal profile of a slope as a result of weathering, of the accumulation of debris in less-steep areas and of the succession of vegetation.

For the analysis of the trajectories of movement, we need to refer to simplified models which are targeted to mirror the natural conditions of a slope as precisely as possible. As a consequence, the geotechnical design of any protection measure relies on a set of numerical experiments which allows to explore different aspects of the phenomenon and to recognize the main factors that affect the motion of fall in a particular situation.

These issues lead to certain modelling uncertainties, therefore, the modelling results should be validated by field observations.

8.1.1.2 GeoRock2D

The two-dimensional rockfall simulations were performed using the GeoRock software which is based on Lumped Mass or C.R.S.P. models (GEOSTRU INDEX 2014). To take the geometry of the boulders (sphere, cylinder or disc) into account, the simulation is processed using the CRSP model (Colorado Rockfall Simulation Program) developed by PFEIFFER and BOWEN (1989). The reliability of the model was verified by comparison between numerical results and those obtained from in-situ tests (GEOSTRU INDEX 2014).

8.1.2 Input data

For the rockfall simulation several input data are required. The underlying geometry of the slope was evaluated by the combination of two digital elevation models (DEM) with different spatial resolution. The available DEM of the riverbed has a resolution of 0.5 m and the DEM of the valley flanks 12 m. As the coarse 12 m resolution lead to uncertainties in the simulation, simulation results have to be interpreted with caution. After merging both DEMs together, cross sections were chosen according to our field interpretation and are used as a basis for the 2D-rockfall simulation. The simulation itself was performed for 30 subsequent repetitions. In the computer simulation, the detachment zone, the actual block geometry, material properties in the transit area and in the deposition area as well as the size of the design block were taken into account. As described in Chapter 4.3, the characteristic design block for a rockfall event at M-D4 was determined with 5.4 m³ and at M-D6 with 8.5 m³. Numerically, this design block was modelled trough a cylindrical shape with the density of 2,650 kg/m³, resulting in a mass of 14,245 kg for M-D4 and 22,487 kg for M-D6, respectively (see Tab. 8-1). The material properties were defined trough roughness parameters obtained during in-situ field investigations.

Tab. 8-1: Boulder characteristics.

	M-D4 t_1	M-D4 t_2	M-D6 t_2
Boulder form	Cylinder	Cylinder	Cylinder
Approx. boulder volume	5.4 m³	5.4 m³	8.5 m³
Density	2,650 kg/m³	2,650 kg/m³	2,650 kg/m³
Diameter	1.95 m	1.95 m	2.45 m
Cylinder height	1.80 m	1.80 m	1.80 m
Mass	14,245 kg	14,245 kg	22,487 kg
Number of simulations	30	30	30

8.1.3 Rockfall hazard zone: M-D4

The area 20 m to 80 m northward the gallery is highly exposed to rockfall activity originating from the adjacent slopes. To determine precisely potential rockfall trajectories the hazardous area (M-D4) was divided into several cross sections. According to our findings from field investigations the following two cross sections were distinguished as potential rockfall trajectories (M-D4 t_1 and M-D4 t_2, see Fig. 8-1 and Fig. 8-2). Trajectory 1 originates from a steep rock wall facing to the south-east. Single rock boulders with a volume of 5.4 m³ were assumed to detach from a solid rock face leading to the red-coloured debris cone visible in Fig. 8-1 on the left. The debris cone is well-sorted starting from fine to coarse material. The lower end of the cone is covered with shrubs. These characteristics were included in the rockfall simulation in terms of roughness and material properties. On the right side of Fig. 8-1 a second debris cone is detectable, originating further north in the valley flank and depositing a large greyish debris cone. In between both debris cones a second trajectory (M-D4 t_2) was assumed to pose a hazard to the road. Both trajectories were evaluated separately in the computer simulation.

Fig. 8-1: M-D4 trajectories 1 and 2; view to NNW.

Fig. 8-2: Satellite image of M-D4 trajectories 1 and 2 (3).

8.1.3.1 Rockfall hazard trajectory M-D4 t_1

A: Simulation <u>without</u> placing a rockfall barrier

The simulation of a single rockfall event at M-D4 t_1 was calculated with the boulder characteristics summarized in Tab. 8-2. The results are visualised in Fig. 8-4. Despite some boulders stopped already on the upper part of the debris cone, others did reach the road and pose therefore a hazard to infrastructure, penstock and the operating staff. In Tab. 7-2 the characteristic values of the design boulder are introduced ((HpMax) Maximum height, (V_{max}) Maximum velocity, (E_{max}) Maximum energy) at the time of impact on the road at position x = 210 m. Additionally, in Fig. 8-3 a histogram of the energy distribution at the position of the road is presented.

Tab. 8-2: Simulation result without placing a rockfall barrier at the position of the road (x=210m).

X_b [m]	Y_b [m]	HpMax [m]	V_{max} [m/s]	E_{max} [KJ]
210	21.05	0.5	9	1,050

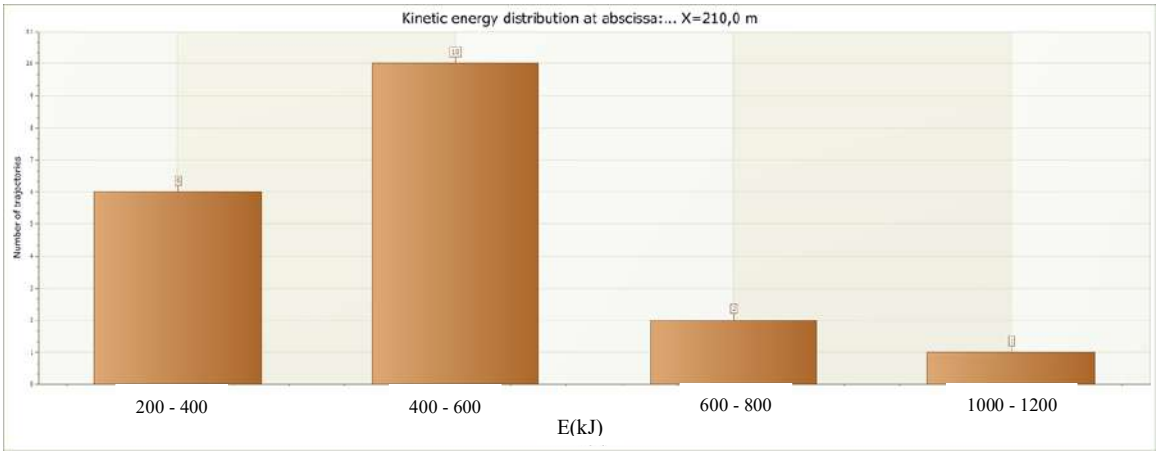

Fig. 8-3: Kinetic energy distribution at the road (x = 210 m)